Front. Earth Sci. 2020, 14(4): 711–737
https://doi.org/10.1007/s11707-020-0821-5

RESEARCH ARTICLE

Responses of a $^{234}U/^{238}U$ activity ratio in groundwater to earthquakes in the South Baikal Basin, Siberia

Sergei RASSKAZOV (✉)[1,2], Aigul ILYASOVA[1], Sergei BORNYAKOV[1,2], Irina CHUVASHOVA[1,2], Eugene CHEBYKIN[1,3]

1 Institute of the Earth's Crust, Siberian Branch of RAS, Irkutsk 664033, Russia
2 Irkutsk State University, Irkutsk 664033, Russia
3 Limnological Institute, Siberian Branch of RAS, Irkutsk 664033, Russia

Abstract In the western part of the South Baikal Basin, spatial-temporal distribution of earthquake epicenters shows quasi-periodic seismic reactivation. The largest earthquakes that occurred in 1999 (M_W = 6.0) and 2008 (M_W = 6.3) fall within seismic intervals of 1994–2003 and 2003–2012, respectively. In the seismic interval that began in 2013, the $^{234}U/^{238}U$ activity ratio (*AR*) in groundwater was monitored assuming its dependence on crack opening/closing that facilitated/prevented water circulation in an active boundary fault of the basin. Transitions from disordered, high-amplitude fluctuations of *AR* values to consistent, low-amplitude fluctuations in different monitoring sites were found to be sensitive indicators of both small seismic events occurring directly on the observation area, and of a large remote earthquake. The hydroisotopic responses to seismic events were consistent with monitoring data on deformation and temperature variations of rocks. The hydroisotopic effects can be applied for detecting a seismically dangerous state of an active fault and prediction of a large future earthquake.

Keywords $^{234}U/^{238}U$, groundwater, earthquake, active fault, Baikal

1 Introduction

Time and place prediction of large earthquakes remains a challenging problem, the solution of which is urgently required for reduction of socio-economic losses from seismic hazards. As a result of intense study, more than 600 phenomena, which preceded and accompanied large earthquakes, have been recognized. Among these, hydrogeological effects play an important role (Johnson et al., 1974; Chia et al., 2008; Shi et al., 2015; Boldina, Kopylova, 2017). In addition to hydrodynamic observations, gas, isotope, and hydrogeochemical data are widely used as signals of large earthquakes and aftershocks in seismically active areas. Radon, He, and Ar contents of groundwater have been measured and shown to change before and after earthquakes (Sobolev, 1993). Other earthquake indicators, such as concentrations of calcium cations (Ca^{2+}), chloride ions (Cl^-), hydrocarbonate ions (HCO_3^-), sulfate ions (SO_4^{2-}), stable isotopes (δD, $\delta^{18}O$, $\delta^{13}C$), variations of hydrothermal temperatures, etc., have been documented (King et al., 1995; Tsunogai and Wakita, 1995; Claesson et al., 2004; Sukhija et al., 2010; Reddy et al., 2011; Li et al., 2019).

An active state of a fault might be defined through measurements of a $^{234}U/^{238}U$ alpha activity ratio (*AR*) in groundwater. Variations of this parameter are explained by excess recoil of ^{234}U into water that is circulated through rocks and minerals impacted by deformation (Cherdyntsev, 1969 and 1973; Chalov, 1975). In this method, chemically separated alpha-emission rates of U isotopes are measured and deviations from equilibrium between ^{234}U and ^{238}U ($^{234}U/^{238}U$ alpha activity ratio = 1, corresponding to an atomic ratio of 5.47×10^{-5}) are used to infer excess recoil.

Zverev et al. (1975) demonstrated an increasing *AR* by a factor of 10 in groundwater after a large earthquake occurred in Georgia. An opposite deformational response to a large seismic event was identified through monitoring of *AR* values in groundwater from the San Andreas Fault in Western USA (Finkel, 1981). In the latter case, a hydroisotopic effect related to a large earthquake was registered in only one of 24 sites associated with Southern California fault zones. Within a year and a half before the Imperial Valley earthquake (M_W = 6.6), the NILA-2W site

Received September 10, 2019; accepted April 9, 2020

E-mail: rassk@crust.irk.ru

showed increasing *AR* values from 2.6 to 5.4. After the earthquake, values decreased to 1.5, followed by return values as high as 5. At the time of the earthquake, U concentrations ([U]) decreased from 0.013 μg/L to 0.0055 μg/L. After the earthquake, the concentration increased to 0.044 μg/L, followed by a return value as low as 0.005 μg/L.

No reasonable interpretation was suggested to explain increasing and decreasing co-seismic fluctuations of a $^{234}U/^{238}U$ activity ratio. Because of the ambiguity of the results, this parameter was not proposed as a reliable earthquake precursor. The negative assessment of its prognostic value was due to both doubtful *AR* results obtained at low [U] and a failure to analyze the relationship between *AR* temporal variations and seismic events.

Subsequently, U-isotope ratios were measured in water samples by thermal ionization mass spectrometry (TIMS) (Edgington et al., 1996; Riotte and Chabaux, 1999; Paces et al., 2002), and by multi-collector inductively coupled plasma mass spectrometry (MC–ICP–MS) (Maher et al., 2006; Chabaux et al., 2011; Wang and You, 2013). Since the development of these approaches, no new attempt has been undertaken to study the Cherdyntsev-Chalov effect in a seismically active fault.

For U monitoring, ICP–MS is examined as highly relevant because it allows rapid measurement of 30–60 samples per day (Goldberg et al., 2001; Halicz et al., 2000; Shen et al., 2002; Cizdziel et al., 2005; Chebykin et al., 2007). This technique provides data on both a $^{234}U/^{238}U$ activity ratio and [U]. Variations of the latter parameter were recorded by this method in groundwater samples before, during, and after the 2009 L'Aquila earthquake (M_W = 6.3) in Italy (Plastino et al., 2011). Spikes in [U] before the earthquake were interpreted as indicators of fluid impulse penetrations from the middle to the upper crust preceding the main shock.

Large earthquakes have historically occurred in the Baikal Rift System, with predictions of future incidents likely (Solonenko, 1974; Sherman, 2014; Map, 2018). Research, in terms of a probabilistic theoretical analysis, indicates a medium-term forecast (Ruzhich, 1997; Sherman, 2009, 2013; Timofeev et al., 2013). Data has shown elastic stress in the crust during earthquakes for the South Baikal area by Radziminovich et al. (2006) and Melnikova et al. (2012). To adequately prepare for a large earthquake, early detection is essential. Timing must be defined by monitoring known precursors, as well as clarifying the character of the evolution and physical nature of the seismic process that precede earthquakes.

In the South Baikal area, earthquakes with an M_W of 5.8 to 7.5 occurred in 1769, 1771, 1779, 1839, 1862, 1866, 1885, 1902, and 1959. During the last two decades, there were two more large seismic events: the 1999 South Baikal earthquake (M_W = 6.0) and the 2008 Kultuk earthquake (M_W = 6.3) (Radziminovich et al., 2006; Melnikova et al., 2012). For practical use, data on earthquake magnitudes are converted into an energy class of *K* using the Rautian formula: $K = 4.0 + 1.8$ M at $K \leqslant 14$ and $K = 8.0 + 1.1$ M, if $K > 14$. For the South Baikal and Kultuk earthquakes, *K* values of 14.6 and 15.9 were defined, respectively (Map, 2018).

The epicenter of the Kultuk Earthquake was 40 km east-southeast of the Kultuk Village. From a spatial shift of aftershocks, seismogenic rupture was inferred to be directed from the main epicenter to the Kultuk area. Therefore, the area was designated as a potential location for a future large earthquake, presumably accommodated in the Main Sayan fault zone (Dobrynina and Sankov, 2008). This prediction was perceived as a threat of a catastrophic event for Irkutsk, with a population of more than 600 000. Both $^{234}U/^{238}U$ activity ratios and [U] were monitored in groundwater samples from the Kultuk area (Fig. 1) to evaluate their usefulness for future earthquake prediction.

In the initial observations from 2012–2013, varying durations and oscillation amplitudes of *AR* values and [U] were detected. Synchronizations of $^{234}U/^{238}U$ cycles in water samples from different sites were observed simultaneously with small seismic events (K = 9–10) that occurred directly in the study area on April 24, 2013 and July 6, 2013. It was inferred that the crust of the Kultuk area was affected by deformations resulting from reactivation of the western end of the Obruchev Fault due to a trigger effect induced from its central part (Chebykin et al., 2015; Rasskazov et al., 2015).

The purpose of this paper is to substantiate a hydroisotopic method for prediction of a large earthquake on the basis of data obtained in the Kultuk area. Spatial-temporal distribution of earthquake epicenters in the South Baikal region are examined with special attention given to those monitored by time: small seismic events of April 24, 2013; July 6, 2013, and March 19, 2014 that occurred in or near the Kultuk area, and the larger earthquake of September 5, 2015 (K = 12.4, M_W = 4.7), with an epicenter 140 km from Kultuk. *AR* variations in groundwater are interpreted and probable scenarios for the generation of a large future seismic event, as well as its prediction through hydroisotopic records, are discussed.

2 The Kultuk area as a key for recent tectonics

The Kultuk area is located between the lacustrine South Baikal Basin and the Tunka Valley (Fig. 1). The basins of the Tunka Valley subsided since the Oligocene, but in the Late Quaternary, the eastern part of the valley, from the Elovka spur to the western extremity of Lake Baikal, was uplifted. Inverse motions in the Elovka-Kultuk section of the valley were caused by compression associated with the

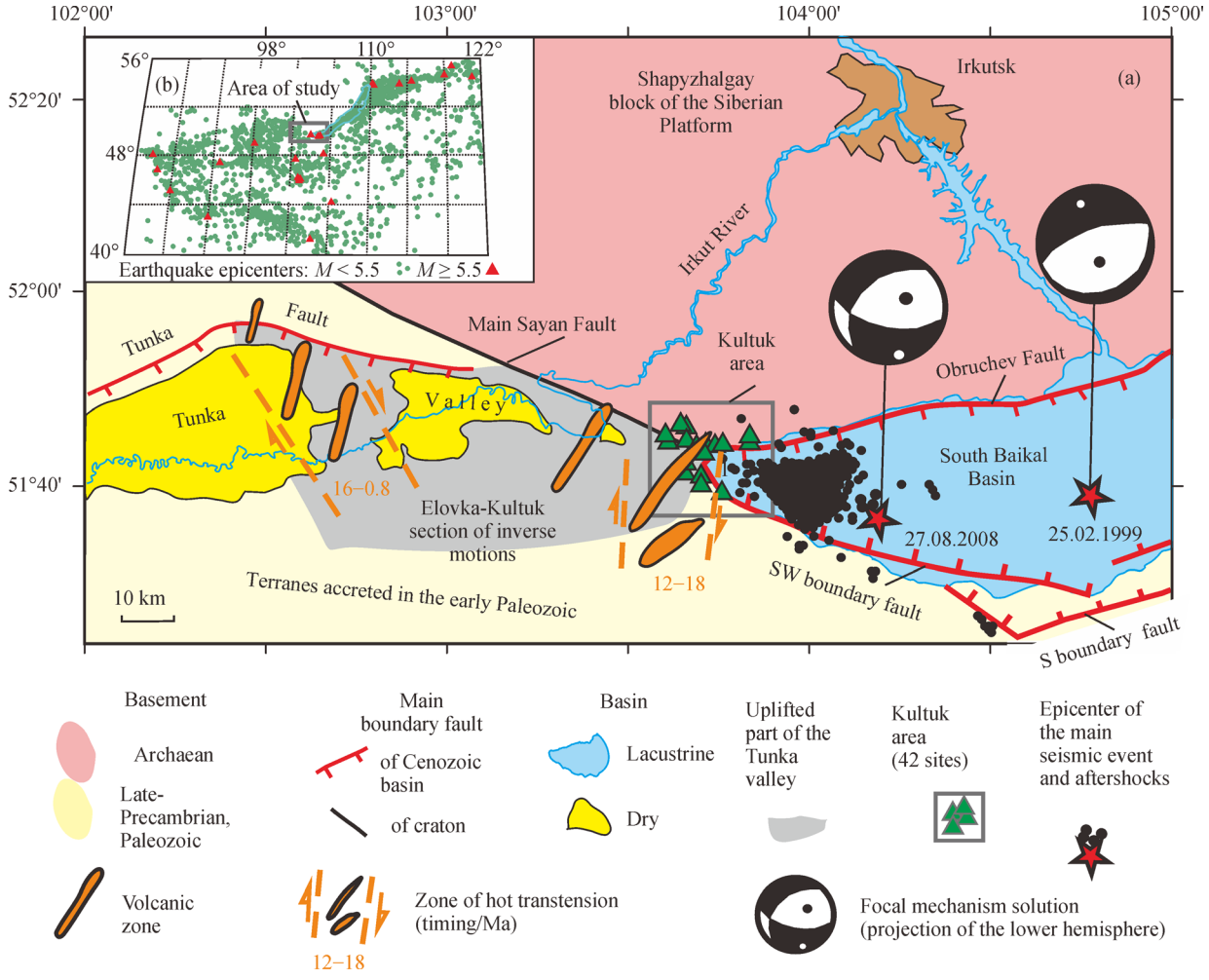

Fig. 1 Spatial position of the Kultuk area for earthquake prediction between the extended South Baikal Basin and compressed inverted area of the Tunka Valley. Panel (a): master faults of the South Baikal Basin are adopted (Florensov, 1968), epicenter and mechanism of the main seismic shock and aftershocks of the 2008 Kultuk earthquake (Melnikova et al., 2012), epicenter of the 1999 South Baikal earthquake (Radziminovich et al., 2006), zones of hot transtension (Rasskazov et al., 2013). Panel (b): earthquake distribution in the Baikal-Mongolian region from 1960–2003 (Sherman, 2014).

development of thrust faults.

The Main Sayan Fault, running from the Kultuk area to the west-northwest, separates a basement of the Siberian platform from adjacent folded terranes that were accreted to the edge of the Siberian continent in the Early Paleozoic (Belichenko et al., 2006). The Holocene paleoseismogenic dislocations of the fault yielded a total estimate of left-lateral displacements up to 30 m (Chipizubov and Smekalin, 1999). However, transverse zones of volcanism, dated at 12–18 Ma, intersect the Main Sayan Fault between Lake Baikal and the Irkut River without notable lateral shift. En-echelon, northeastern lines of volcanoes and dikes define the north to south, hot Kamar-Stanovoi transtension zone. Motion along this zone is focused at the Main Sayan Fault and is consistent with compression along the western flank of the transtension zone (i.e., the Elovka-Kultuk section of the Tunka Valley), extending into its eastern flank (i.e., the western part of the South Baikal Basin) (Rasskazov et al., 2013). Unlike the 1999 South Baikal earthquake, which marked the normal fault activity, the 2008 Kultuk event revealed a lateral component.

Rapid Neopleistocene-Holocene subsidence yielded the deep basin now occupied by Lake Baikal (Logatchev, 1974). Seismic profiles (Hutchinson et al., 1992) showed sub-horizontal bottom sediments in the western part of the South Baikal Basin. This pattern of a rift structure differs from those that are asymmetrical, which are characteristic in the eastern part of the South Baikal Basin, as well as the Tunka, Barguzin, and other rift valleys (Logatchev, 1974). Consequently, lake subsidence in the western part of the South Baikal Basin is equally accommodated by the northern and southern boundary faults.

The Basin is bounded on the north by the Obruchev Fault and on the south by the southwestern (SW) and

southern (S) boundary faults. The Obruchev Fault extends from Kultuk Village in the west to Buguldeika Village in the northeast. This fault consists of the western and northeastern fragments. The western fragment stretches from west to east and continues eastward to the lake as a structural line, by which the intra-basin uplift of the Posol'skaya Bank has become isolated (Logatchev, 1974; Hutchinson et al., 1992; Levi et al., 1995). The northeastern fragment extends northeast. The S boundary fault consists of coastal and sub-aqueous sections. The former separates the intermediate Tankhoi tectonic step from the Khamar-Daban range while the latter separates the step from the bottom of the lake (Fig. 2).

3 Earthquake distribution

Recent seismicity has primarily been concentrated within a lake area. The western fragment of the Obruchev Fault limited earthquakes in the north. The southwestern continuation of the northeastern fragment of the Obruchev Fault is marked by earthquake epicenters, although it does not show an explicit expression in morphology of the lake bottom. Beyond the basin boundaries, the seismically active area splits into the Sayan and Khamardaban epicenter branches. The former exhibited only four small earthquake events between March 22, 1995 and February 10, 1999 (i.e., before the 1999 South Baikal Earthquake); the latter displayed multiple events in the subsequent time interval between February 25, 1999 and July 3, 2015.

From 1996 to 2008, seismic intervals of 23–28 and 63–87 months were characterized with the major events of the energy classes K = 12.2–12.4 and 14.6–15.9. These intervals were separated from each other by aseismic intervals of 10–13 months. A large earthquake occurred 15–16 months after the beginning of each seismic interval. Earthquake epicenters of a high energy class (K = 12.2–15.9) migrated into the western part of the lake (events of 1996, 1999, 2005, and 2008). However, the successive migration stopped. The earthquake of September 5, 2015 (K = 12.4) occurred near the northeastern fragment of the Obruchev Fault (Fig. 2(a)). Additionally, earthquakes of elevated magnitude ($M \geqslant 4$) were characteristic of the western fragment of the Obruchev fault and in the SW boundary fault in the time interval of 1996–2008. After the 2008 Kultuk Earthquake, those of elevated magnitude occurred only in the northeastern fragment of the Obruchev Fault (Figs. 2(b) and 2(c)).

Intervals between earthquakes of K = 12.2–12.4 and K = 14.6–15.9 lasted 36 and 41 months, respectively, from 1996–1999 and 2005–2008. If repeated seismicity is quasi-periodic, the next seismic shock of K = 14.6–15.9 should be expected during 2019–2020. The hypothesis for the evolution of seismicity from 1994 to 2012, within two cycles (Fig. 2(b)), assumes a separation of the cycles by an aseismic interval as long as 10 months (between January 1 and November 16, 2003), with a launch of the second cycle in the fall of 2003.

4 Seismic reactivations

At the beginning (November 16, 2003–October 12, 2004), earthquakes were sparse and dispersed in lake areas along its southern and northern coasts. During this time, there were no events of $K > 9.8$. The spatial-temporal epicenter sequence yielded an ellipse locus with clockwise migration. From 2005 to 2006, the major earthquake of March 21, 2005 (K = 12.2) was marked by an epicenter in the central part of the lake area. Over time, the epicenters migrated from the lake to its southern coast (Fig. 3(a)).

The 2007–2008 Snezhnaya reactivation was exhibited by several earthquakes with the maximal energy class K = 10.1. In the interval between February 12 and December 6, 2007, earthquakes along the northeastern bend extended from the Koty to Snezhnaya epicenter clusters. Then, between January 1 and May 4, 2008, epicenters migrated westwards with the final event (K = 10.1) at the western extremity of the lake on May 4, 2008 (Fig. 3(b)).

The Kultuk reactivation began with the Kultuk Earthquake that occurred after a seismic quiescence of 115 days. Epicenters of aftershocks were distributed both in the lake and on its southern coast. On background of dispersed and disordered earthquake distribution, the Kultuk, Vydrino, and Koty epicenter clusters were clearly displayed (Fig. 3(c)).

After the largest reactivation of 2008–2010, almost seven months passed before the Tolbazikha reactivation of 2011–2012 started. From June 24 to October 19, 2011 earthquakes were localized in South Baikal near the Tolbazikha Village. Subsequently, from March 16 to October 11, 2012, they were dispersed in the form of a fan that opened westwards from the northern to the southern coasts of Lake Baikal. Earthquake epicenters consistently migrated with oscillating (pendular) clockwise rotation around the Tolbazikha epicenter cluster. The epicenter of the final event of reactivation was in the central part of the lake area. In this reactivation, there were two earthquakes with a maximum energy class K = 10.4: one with an epicenter on the southern shore of the lake on August 14, 2012, followed by a second 12 days later with an epicenter near the Obruchev Fault. The first earthquake did not fit into the sequence of oscillating rotation; the second was one of the links in this sequence. An earthquake on June 14, 2012 in the Kultuk area: 1) preceded the major events of this seismic reactivation, 2) was an intermediate link between rotational migration from the event of March 16, 2012 to the major event of August 26, 2012, and 3) reflected radial shift of epicenters from the Tolbazikha epicenter cluster to the Kultuk area

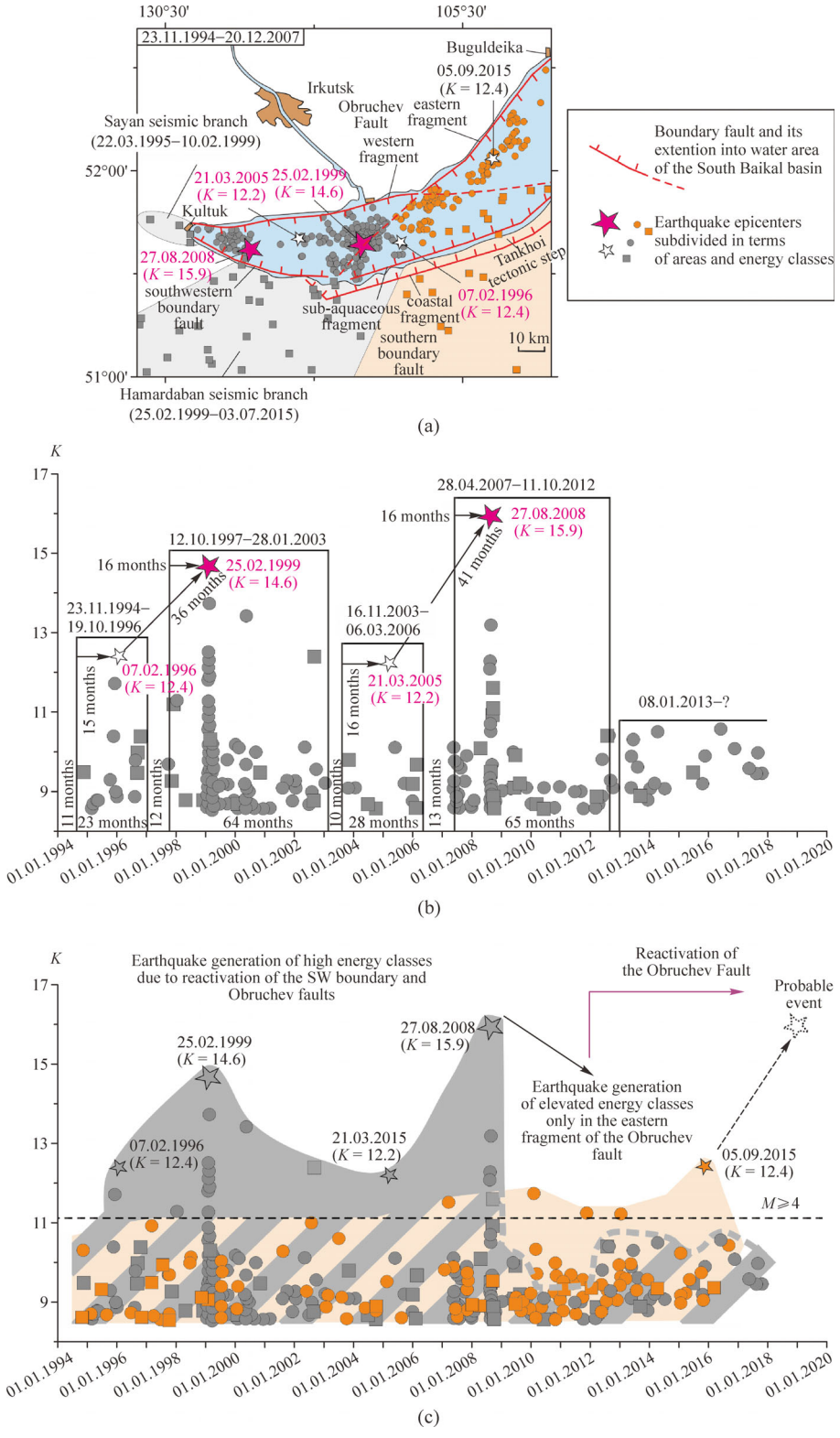

Fig. 2 Seismicity of the South Baikal Basin and coast from 1994–2017 (data from the catalog of the Baikal Branch of the Geophysical Service of the SB RAS (Map, 2018)). (a) – distribution of earthquake epicenters; (b) – a sequence of seismic events of different energy classes with subdivision into reactivations of strong earthquakes (K = 12.2–15.9) in the western part of the South Baikal Basin; (c) – transition from a generation of earthquakes ($M \geqslant 4$) in the SW boundary fault and western part of the Obruchev Fault to their generation in the northeastern part of the Obruchev Fault. The spatial separation of earthquake epicenters, shown by different symbols on panel (a), is presented in a grouping of earthquakes with different energy classes on panels (b) and (c).

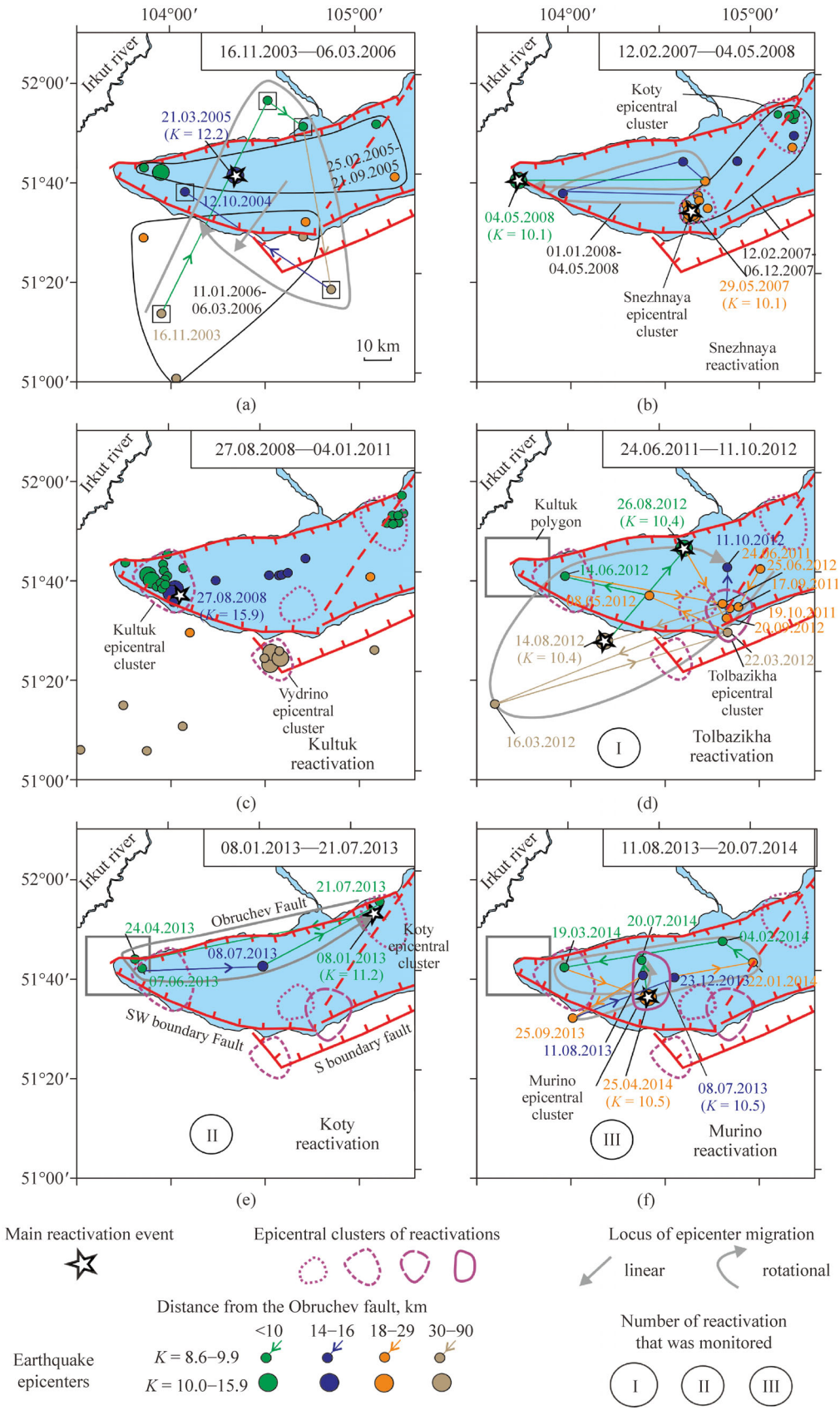

Fig. 3 Distribution of earthquake epicenters in the western part of the South Baikal Basin and adjacent coast in 2003–2014. Symbols as in Fig. 1.

and back (Fig. 3(d)).

The Koty reactivation of 2013 differed from the one of 2011–2012. It started with a major earthquake on January 8, 2013 ($K = 11.2$) at the Koty epicenter cluster, followed by seismic events at the Kultuk area. The next earthquake on July 8, 2013 ($K = 10.3$) occurred in the center of a lake, followed by the final occurrence on July 21, 2013 at the Koty epicenter cluster. This seismic reactivation exhibited the only pendular move from the Koty cluster to the Kultuk area and back. Unlike the Tolbazikha reactivation, the Koty reactivation was characterized by a counter-clockwise rotation of epicenters that were closely related to the western fragment of the Obruchev Fault (Fig. 3(d)).

The Murino reactivation of 2013–2014 was expressed by earthquakes that successively migrated with an oscillating (pendular), counter-clockwise rotation around the Murino epicenter cluster that involved a main shock occurring on April 25, 2014 ($K = 10.5$) (Fig. 3(e)).

After a 12-month aseismic gap during 2014–2015, sparse earthquakes related to the reactivated northeastern fragment of the Obruchev Fault first occurred (from January 13, 2015 to August 29, 2016) at the Goloustnoe and Koty epicenter clusters. The major event occurred on September 5, 2015 ($K = 12.4$) in the former cluster. Subsequently, epicenters shifted to the center of a lake from December 14, 2016 to November 10, 2017. Similar shifts in the locus of earthquake epicenters occurred from February 12 to December 6, 2007. The band of epicenters stretched from Peschanaya Bay (the epicenter cluster of the Obruchev Fault) to the subaqueous portion of the Snezhnaya River Delta (the epicenter cluster at the junction between the SW and S boundary faults). This epicenter locus preceded the seismicity that migrated to the Kultuk Village from January 1 to January 31, 2008 to an event on May 4, 2008 near the village, finalized by the large Kultuk Earthquake on August 27, 2008.

From the first earthquake of the Koty reactivation on January 8, 2013 until the next large earthquake, seismicity developed over 5 years, similar to the stages A, B, C, and D of the Kultuk Earthquake, which lasted 3 years and 2 months. In both cases, stages A and B occurred during the initial 1.5 years, and stage C began approximately 2 years after onset of stage A (respectively, in early 2007 and 2015). Subsequently, stage C of a large earthquake build-up lasted 1.5 years longer than the respective stage C of the Kultuk Earthquake build-up. The new stage D may also be longer than the respective stage D of the previous Kultuk earthquake build-up. If so, a future large earthquake could occur in 2019–2020, as inferred from data shown in Fig. 2. An additional complication of the build-up of a new large earthquake is the division of its stage D into phases D1 and D2 expressed in the distribution of earthquakes along the Koty-Murino and Listvyanka-Posol'skaya Bank lines (Table 1, Fig. 4).

While analyzing the west to east distribution of earthquake epicenters (Fig. 5), the occurrence of sparse events is emphasized in 2003–2004 and 2015–2017. In the former, the epicenters were dispersed, while in the latter, they were concentrated along the Goloustnoe–Murino line, spatially related to the Obruchev Fault.

Highlighting the role of major event epicenters and epicenter clusters in every seismic reactivation, one can see their distribution in the Snezhnaya, Kultuk, and Tolbazikha reactivations of 2007–2012 along the northern and southern boundary faults of the South Baikal Basin. The area of the major seismic events was the largest in the Snezhnaya and Kultuk reactivations. The area was reduced in the Tolbazikha reactivation with the subsequent transition to the narrow linear epicenter zone of the Koty reactivation in front of the western fragment of the Obruchev Fault, and to the Goloustnoe-Murino locus in front of both the western and northeastern fragments of the fault (Figs. 6(a) and 6(b)).

In all, the seismic reactivations of 2003–2014 exhibit three types of spatial-temporal patterns of earthquake epicenters: 1) spatial shift of clusters (sometimes with pendular migration), 2) chaotic, and 3) rotational (sometimes with pendular migration). These patterns of seismic

Table 1 Comparison of build-up stages for the Kultuk and probable future large earthquakes

Stage of build-up	Characteristics and timing	
	Kultuk Earthquake of August 27, 2008	Probable future earthquake of 2019–2020
A	Reactivation of the western fragment in the Obruchev Fault (February 25–September 21, 2005)	Koty reactivation (January 8–July 21, 2013)
B	Development of seismic processes in the Khamardaban land branch (January 11–March 6, 2006)	Murino reactivation within inundated area of the lake (August 11, 2013–July 20, 2014)
C	Peschanaya-Snezhnaya epicentral band (February 12–December 6,2007)	Activity of the Goloustnoe and Koty epicentral clusters (January 13, 2015–August 29, 2016)
D	Migration of epicenters from the Snezhnaya cluster to the Kultuk Village and back with clockwise rotation (January 2–31, 2008), individual earthquake near the Kultuk Village (May 4, 2008)	Phase D1: activity of the Murino part of the Goloustnoe-Murino epicentral line (December 14, 2016–October 10, 2017), phase D2: activity of the Listvyanka–Posol'skaya Bank epicentral line (March 16–July 31, 2018), probable additional events (2020 or later)

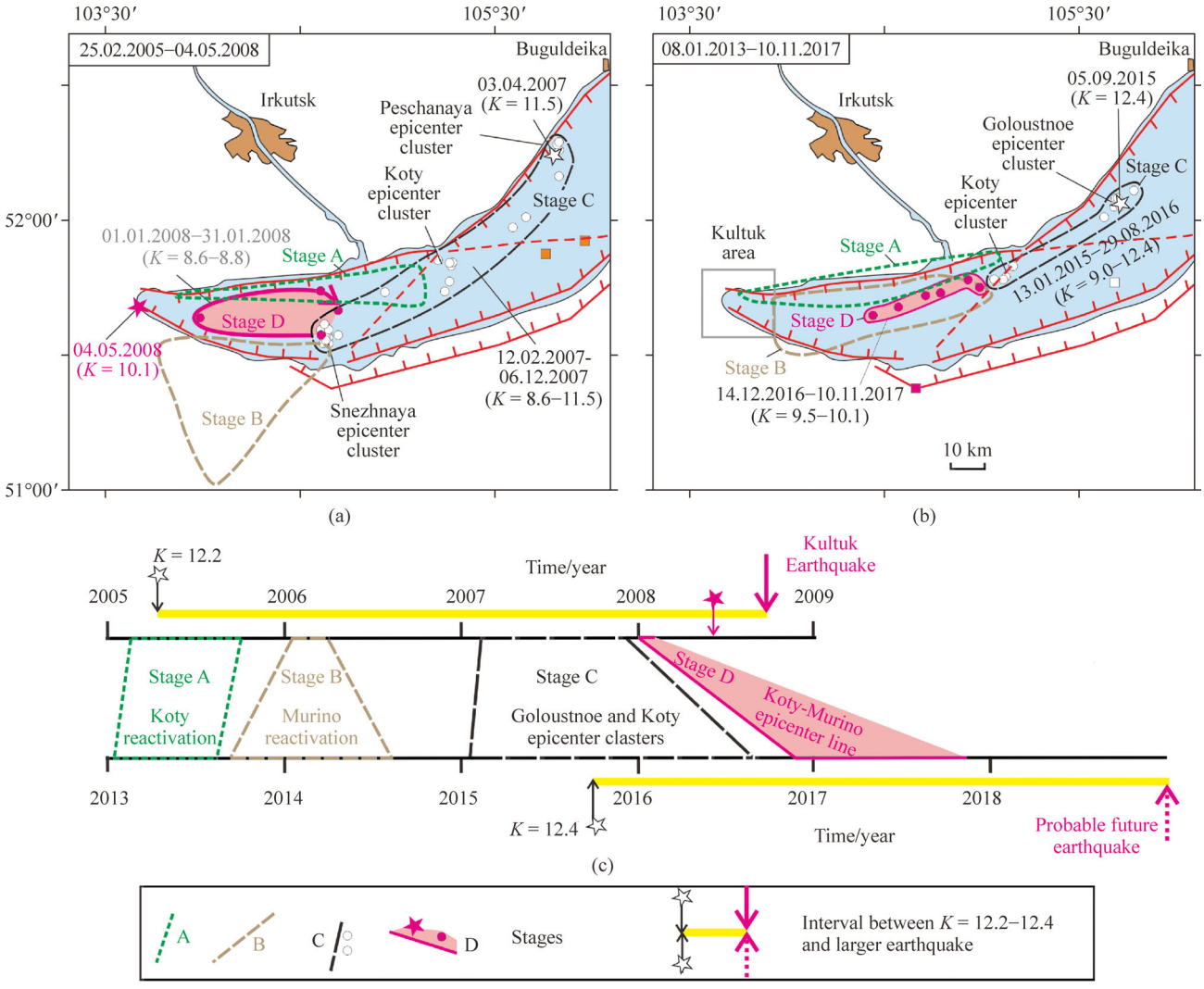

Fig. 4 Comparisons of spatial-temporal patters of earthquake epicenters related to build-up of the Kultuk and probable future earthquakes. Symbols as in Fig. 2. (a) – stages A–D (Table 1); (b) – similar stages of a probable future large earthquake; (c) – stage correlation on time scale.

activity are referred to as stages A–D of a large earthquake build-up (Fig. 4). Epicenters shifted to the south (2005–2006), the west (2007–2008), and to the west-southwest (2015–2017). Chaotic distribution was characteristic of the 2008–2010 aftershocks of the Kutuk Earthquake. Earthquakes rotated with pendular migrations in the subsequent reactivations of 2011–2012, 2013, and 2013–2014. In each reactivation of 2003–2014, seismic events took place in or near to the Kultuk area (Fig. 5). During the hydroisotopic monitoring of 2012–2014, earthquakes occurred on June 14, 2012 (Tolbazikha reactivation), April 24–June 7, 2013 (Koty reactivation), and March 19, 2014 (Murino reactivation).

Sampling of groundwater was initiated in the Kultuk area two weeks after the June 14, 2012 earthquake of the Tolbazikha reactivation. The six-year monitoring covered the second half of the Tolbazikha reactivation (2012–2013), the Koty reactivation (2013), the Murino reactivation (2013–2014), and the subsequent seismicity along the Goloustnoe-Murino line.

5 Monitoring sites and analytical techniques

Among 42 drill holes and springs, seven were selected for permanent hydroisotopic monitoring. Five monitoring sites (8, 9, 27, 40, and 38) consisted of 120 m deep wells in the Kultuk Village, one (14k) was a spring, and another (11) was a water intake from Lake Baikal. Sites 9, 8, and 27 were located along the Obruchev Fault, site 38 at the SW boundary fault, and sites 40 and 14k at local paleoseismogenic dislocations of the Main Sayan Fault. The water intake site (11) primarily reflects the composition in the

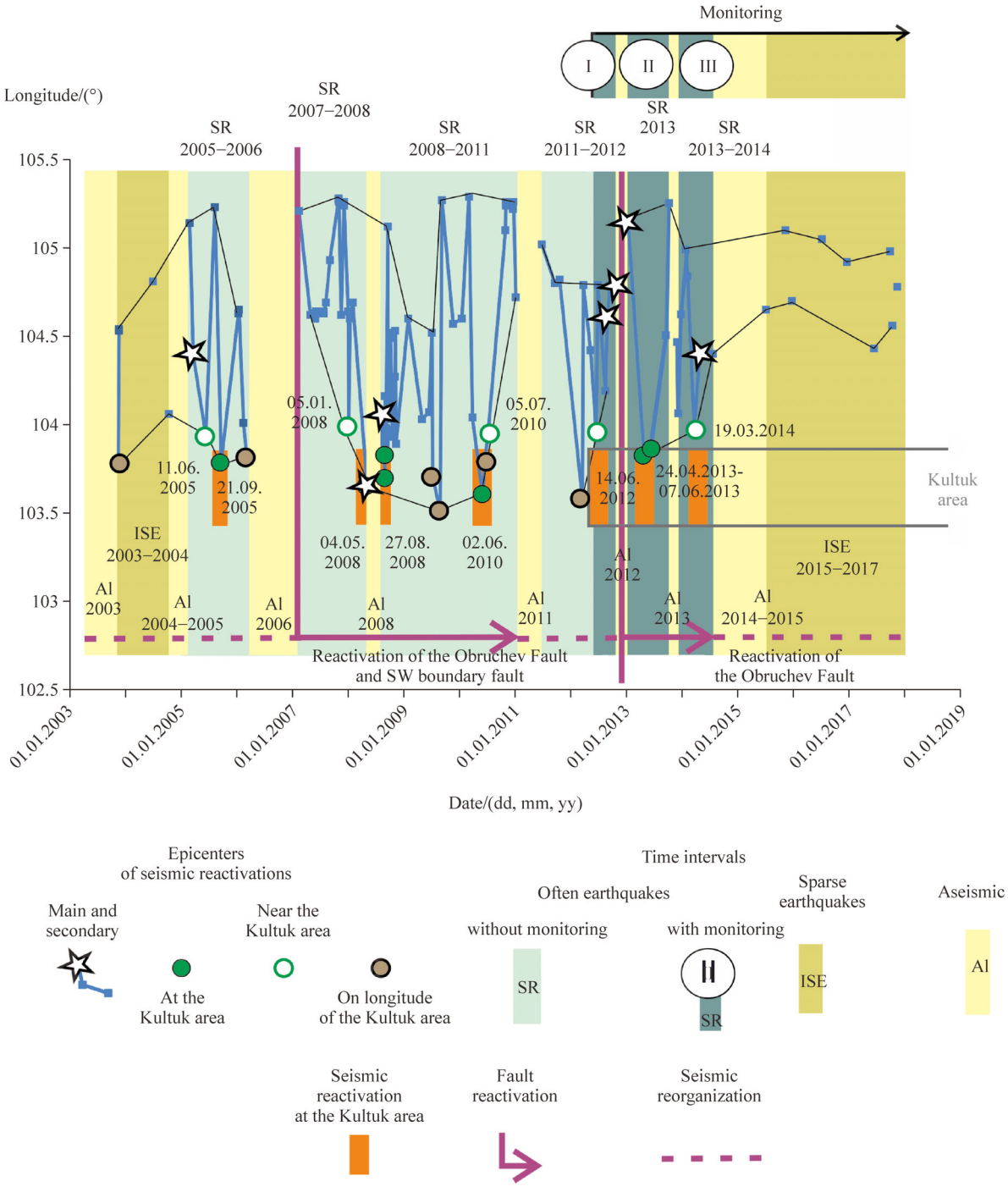

Fig. 5 East–west distribution of earthquake epicenters relative to the Kultuk area. Intervals of seismic reactivation (SR) and those of sparse earthquakes (ISE) are separated by aseismic intervals (AI). Roman numerals from I to III within circles indicate the Tolbazikha, Koty, and Murino seismic reactivations, respectively, during which monitoring was conducted with registration of small earthquakes in the Kultuk area. Data points to the east of longitude 105.5 grades are not shown.

littoral zone of Lake Baikal, with an admixture of a component entering from the Obruchev Fault. In this paper, we present results of hydroisotopic monitoring in sites 8, 9, and 27, located in the Obruchev Fault. For comparisons, we integrate results of hydroisotopic monitoring of site 14k and data of deformational and temperature monitoring of rocks in the Talaya adit (Figs. 7–9).

Samples were collected over a one to three week period. In 2014, intervals between samples were reduced to four days. For analysis, a volume of 0.5 L of water was

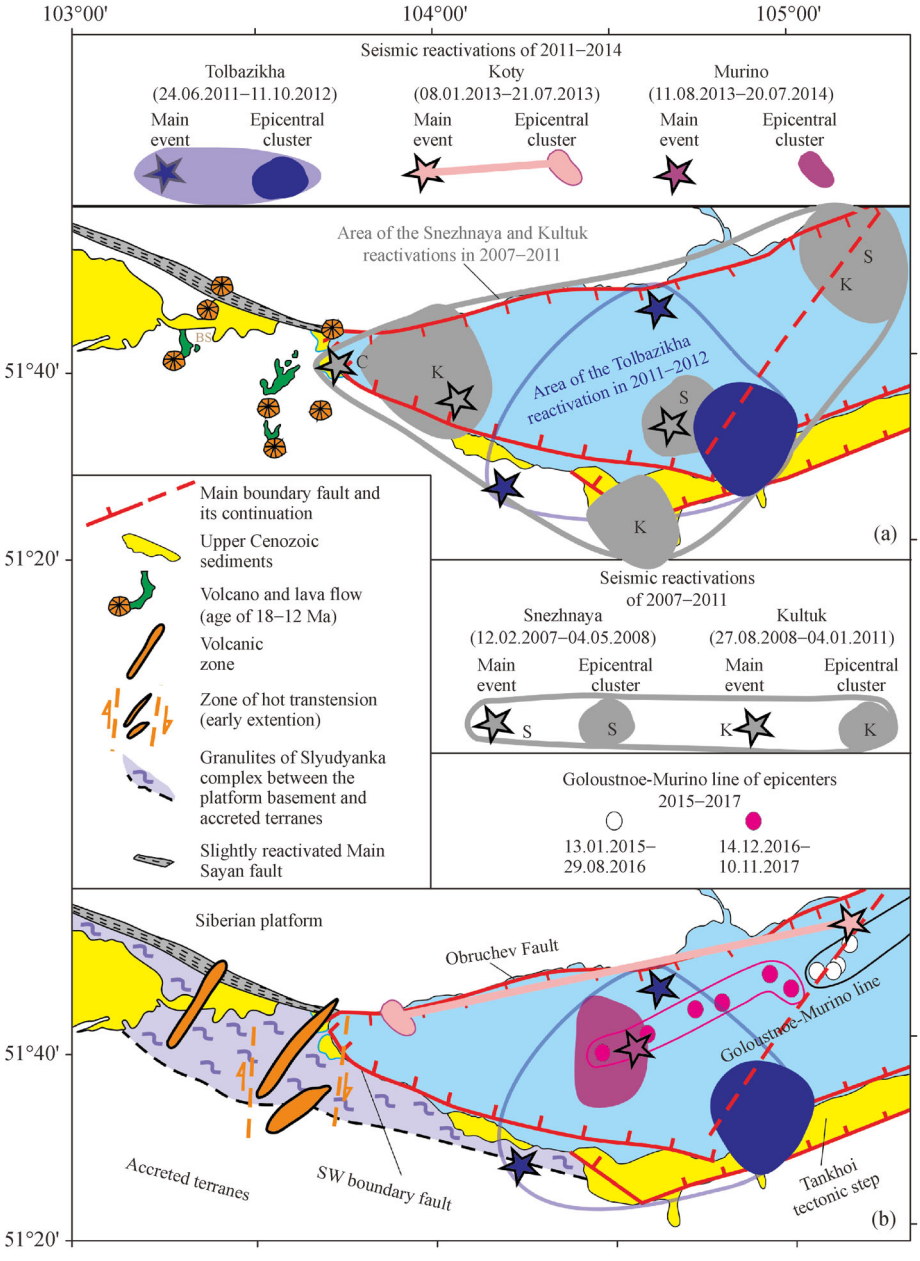

Fig. 6 Synthesis of data on spatial-temporal evolution of seismicity in the western part of the South Baikal Basin before and after the Tolbazikha reactivation that finalized the 2003–2012 seismic interval. Panels (a) and (b) show locations of the two major epicenters and an epicenter cluster of the Tolbazikha reactivation relative to preceding (a) and subsequent (b) epicenter characteristics. Scheme a demonstrates repeated triple combinations of major epicenters and epicenter clusters in the Snezhnaya, Kultuk, and Tolbazikha reactivations, spatially connected with both the northern and southern master faults of the basin. Scheme b shows the transition from the triangular distribution of epicenters in the Tolbazikha reactivation to the linear distribution of epicenter clusters during the Koty reactivation, followed by the Goloustnoe-Murino epicenter line (the north-eastern extension of the line shown in Fig. 4). The SW boundary fault of the South Baikal Basin extends along granulites of the Slyudyanka metamorphic sub-terrane. The fault that inherits this zone is in discordant relations with the S boundary fault, along which the intermediate Tankhoi tectonic step was separated from both the raised Khamar-Daban Range and the subsided bottom of Lake Baikal. The southwestern underwater extension of the northeastern fragment of the Obruchev Fault traces the probable boundary of the Sludyanka metamorphic sub-terrane. The boundary of the granulite metamorphism zone is shown after Shafeev (1970).

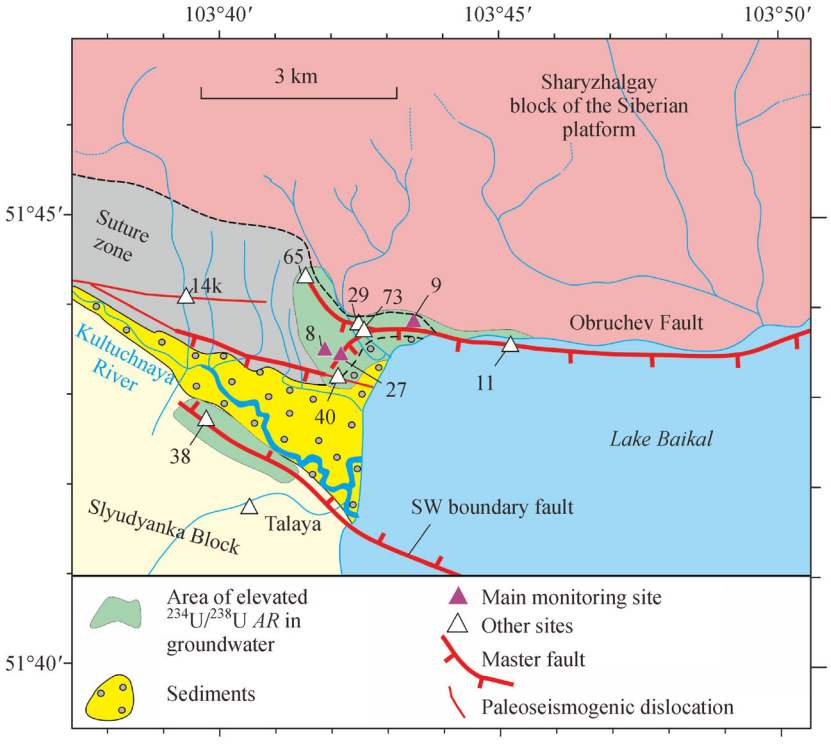

Fig. 7 The Kultuk area for earthquake prediction. Areas of elevated *AR* values in groundwater are highlighted (Rasskazov et al., 2015). Paleoseismogenic dislocations in the Main Sayan Fault zone are shown (Chipizubov and Smekalin, 1999).

collected into a bottle of polyethylene terephthalate (PET). A factory-sealed bottle of deep Baikal water with dissolved solid concentration as low as 100 mg/L was opened just before sampling, emptied, and then thoroughly rinsed with sampled water. If short-term storage (up to three months) was required, selected samples were passed through membrane filters (0.45 μm) and acidified with nitric acid that was distilled twice using the Savillex DST-1000 sub-buffering system. Samples were refrigerated.

U concentrations were determined using the ICP-MS method on an Agilent 7500 ce quadrupole mass spectrometer. To assess measurement errors of [U], we used an experimentally determined dependence of relative standard deviation (RSD %) on the value of the analytical signal *N*: $RSD\% = 125.71 \times N^{-0.3310}$, where N = 20–20000 imp/s. Signals with values > 20000 imp/s, 20000–20, and < 20 imp/s were characterized by *RSD* of 5%, 5%–50%, and > 50%, respectively. The typical measurement errors, depending on element concentrations, are presented in Table 2.

Table 2 Typical errors of [U] measurements using an Agilent 7500ce quadruple ICP-MS spectrometer

Element concentrations in measured solutions/(μg·L^{-1})	< 0.001	0.001–0.1	0.1–1	> 1
RSD/%	> 25	25–10	10–5	5

To determine the isotope composition of U in natural water, U was separated with ion exchange resin TRU Resin-B (50-100μm, Triskem Int., France) using polypropylene columns containing 0.5 mL of TRU resin. Uranium was eluted with 1.5 mL of 0.1 mol/L ammonium oxalate $(NH_4)C_2O_4$. The elutants were diluted 2-fold with 3% HNO_3 and analyzed according to methods developed earlier (Chebykin et al., 2007). Analyses of U isotopes were performed using the ICP-MS method on an Agilent 7500 ce quadrupole mass spectrometer. To control the quality of measurements, a standard sample of the isotope composition of natural U GSO 7521-99 (Urals Electrochemical Plant, Novouralsk) was used. Details of error calculations in the determination of isotope ratios were presented by Chebykin et al. (2015). A typical error (1σ) was approximately 1% relative to a measured value.

Along with $^{234}U/^{238}U$ activity ratios, the $^{87}Sr/^{86}Sr$ ratio was used to evaluate groundwater sources. Strontium was separated from water samples using a simplified procedure (Pin, Zalduegui, 1997). A sample of filtered and acidified water (10 to 50 mL, depending on Sr concentration) was evaporated; 1 mL of 2 mol/L HNO_3 was then added and evaporated to dryness. After addition of 2 mL of 2 mol/L HNO_3, the solution was passed through an ion exchange column filled with 83 mg of Sr Resin-B (50–100 μm, Triskem Int., France). After an addition of 0.5 mL of 3 mol/L HNO_3, Sr was eluted from the resin with a weak

solution of nitric acid (0.05 mol/L HNO_3). Strontium isotope ratios were measured on a Finnigan MAT 262 mass spectrometer. All data were corrected for mass fractionation assuming exponential fractionation behavior and assuming that $^{86}Sr/^{88}Sr = 0.1194$. A standard sample of NBS 987 was used to control the quality of measurements. During the measurement of Sr isotope ratios, the value of the standard sample was 0.710248 ± 0.000013.

The method of deformational and temperature monitoring was described by Bornyakov et al. (2015, 2017).

6 Grouping groundwater site samples

After a long aseismic gap from 2014 to 2015, no seismic events were recorded in the vicinity of the Kultuk area (Fig. 6). Thus a detailed analysis of *AR* variations in connection with earthquake occurrence in the area was limited to a time interval from 2012 to 2014. By grouping data points on the $^{234}U/^{238}U$ *AR* vs. 1/U diagram, approximately five to nine episodes, with different U compositions in groundwater, were distinguished in the selected sites (Fig. 8).

In each of the three reactivations, temporal series of groundwater parameters yielded four extreme components. In the second half of the Tolbazikha reactivation, samples taken in sites 8 and 9 show the following components: I_1: the most enriched with ^{234}U; I_2: the highest 1/U value (minimum [U]); I_3: the least enriched with ^{234}U; and I_4: the lowest 1/U value (maximum [U]). Data points of this reactivation were located within a field enclosed between the extreme components I_1, I_2, I_3, and I_4. Similarly, extreme isotopic and elemental components of the selected sites were allocated for the Koty and Murino seismic reactivations. Deformational changes in the groundwater supply system were reflected in relative shifts of data fields: I_1–I_2–I_3–I_4 → II_1–II_2–II_3–II_4 → III_1–III_2–III_3–III_4.

A monitoring interval from July 31, 2012 to September 21, 2014 of site 9 yielded nine episodes (Fig. 8(b)). The two initial episodes marked the final stage of the Tolbazikha reactivation and transition to an aseismic lull of 2012–2013, the third and fourth marked the transition from the aseismic lull to the Koty reactivation, the fifth, the transition from the Koty to the Murino reactivation, while the sixth to the ninth marked the evolution of the Murino reactivation and the transition to an aseismic gap from 2014 to 2015. The first episode showed a low *AR*, and the second was characterized by elevated ratios. The third and fourth episodes began with elevated *AR* values; the third gave a complete series of mixing between components II_1 and II_3, and the fourth produced a scatter of data points along the abscissa axis and designated components II_2 and II_4. The fifth episode was characterized by relatively expanded variations of isotopic and elemental parameters. The sixth was distinguished by a subdivision of a data set into two contrasting groups with elevated and lower *AR*, displaying a new component III_1. In the seventh and eighth episodes (before the earthquake of March 19, 2014), component III_1 gradually decreased with increasing III_3 (i.e., cracks closed) under a limited range of [U]. In the ninth episode (after the earthquake of March 19, 2014), the elemental components III_2 and III_4 broadly varied without changes of the isotopic components III_1 and III_3.

During the same observation interval, site 8 was subdivided into seven episodes with different isotopic and elemental signatures of U in groundwater (Fig. 8(a)). The first episode, which occurred at the final stage of the Tolbazikha reactivation, marked a trend parallel to the ordinate axis. The second marked the aseismic lull of 2012–2013 and Koty reactivation, indicating a similar *AR* range and increasing 1/U relative to the data field of the previous reactivation. This episode had a trend of weak mutual correlation between isotopic and elemental parameters of U. The third, which corresponded to the initiation of the Murino reactivation, displayed data points within the data field of the Koty reactivation. The fourth to seven episodes were informative for the evolving Murino seismic reactivation and subsequent transition to aseismic lull. The fourth episode was distinguished by a sufficient release of U (component III_4). The fifth revealed component III_1, from which decreasing *AR* and increasing 1/U progressed. The sixth episode (before the event of March 9, 2014 near the Kultuk area) demonstrated a correlation between *AR* and 1/U values. The seventh (after the event on March 19, 2014) yielded a new mixing trend between the components III_2 and III_3, with correlated *AR* and 1/U values.

Unlike sites 8 and 9, site 27 was not involved in sampling during the Tolbazikha reactivation. For the Koty and Murino reactivations, nine episodes with different U compositions of groundwater were identified (Fig. 8(c)). The two initial episodes belonged to the Koty reactivation; the third to the transition from the Koty to Murino reactivation; the fourth to eighth to the evolved Murino reactivation and subsequent aseismic lull of 2014–2015. In the groundwater of site 27, an *AR* was elevated and a 1/U was reduced during episodes of the Koty reactivation. At the beginning of the Murino reactivation, an *AR*, with an approximate correspondence to the maximum values of the Koty reactivation (i.e., the end member II_1), was recorded. Data points of the third (transitional) episode yielded a trend toward components III_1 / III_2. A shift of the isotopic composition indicated an initiation of mixing between the III_1/III_2 and other components of groundwater (III_3 and III_4) that were characteristic of this site during the Murino reactivation. Similar mixing was displayed during the entire fourth episode (from February 1 to May 20, 2014), including the March 19, 2014 seismic event that occurred near the Kultuk area. The fifth episode was characterized by the release of U (with elemental component III_4), the

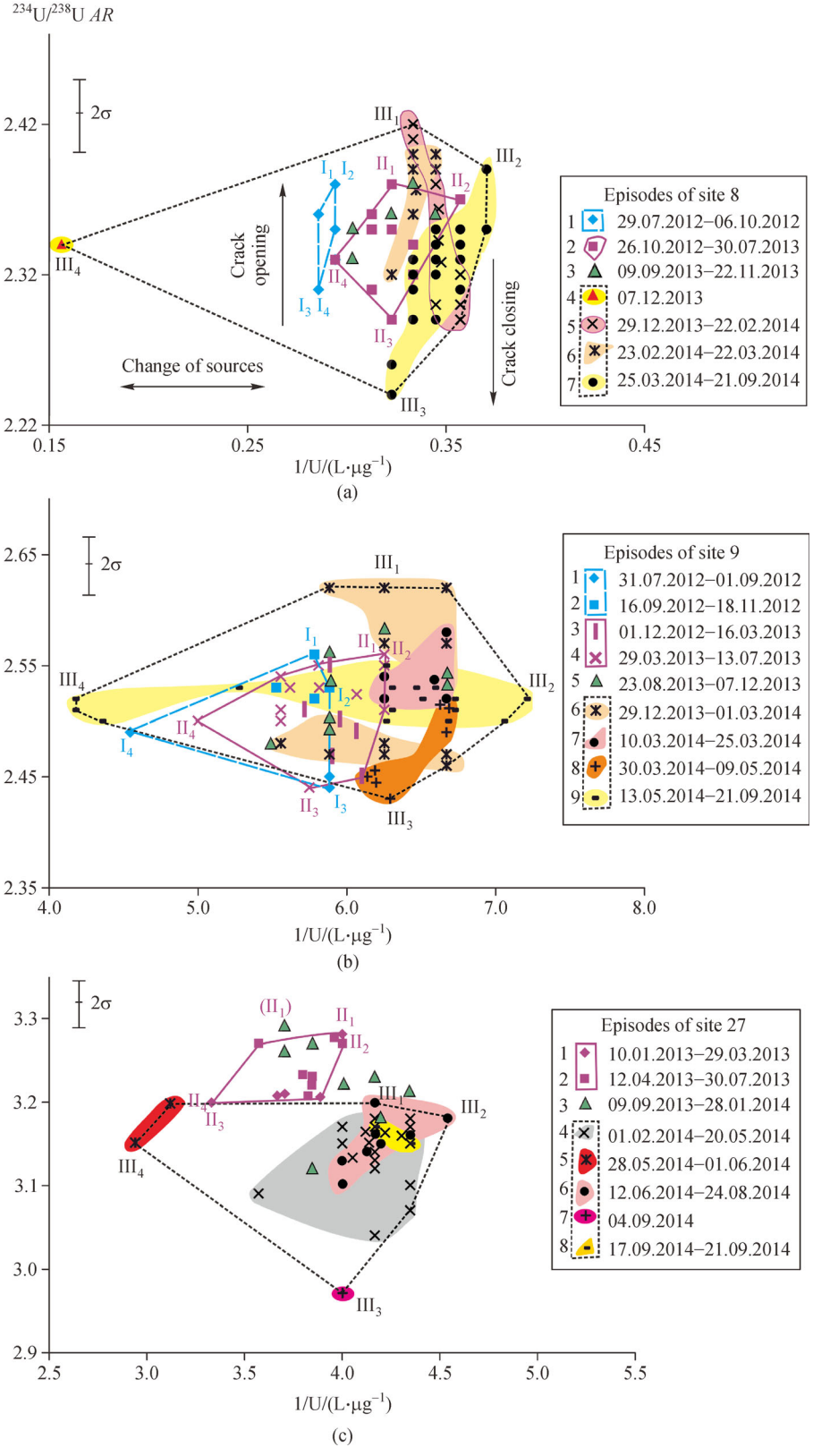

Fig. 8 Temporal variations of $^{234}U/^{238}U$ *AR* vs. 1/U in groundwater from sites 9 (a), 8 (b), and 27 (c) in the context of seismic activity in the western part of the South Baikal Basin (explanations in the text). The Tolbazikha reactivation: site 9 – episodes 1–2, site 8 – episode 1; the Koty reactivation: site 9 – episodes 3–4, site 8 – episode 2, site 27 – episodes 1–2; initial stage of the Murino reactivation: site 9 – episode 5, site 8 – episode 3, site 27 – episode 3 (transitional from the component II_1 of the Koty reactivation, designated as (II_1), to components III_1 and III_2 of the Murino reactivation); middle and final stages of the Murino reactivation: site 9 – episodes 6–9, site 8 – episodes 4–7, site 27 – episodes 4–8.

sixth by a return to a state of the fourth episode (with the elemental component III_2), the seventh by the maximal decrease of an *AR* (with the isotopic component III_3), and the eighth by a return to a state of the fourth episode.

In the transition from the Koty to the Murino reactivation, monitoring sites showed different temporal variations of *AR* and 1/U values. Both were characterized by an increasing variation of both isotopic and elemental parameters; however, each site yielded individual patterns. Data points of the transitional episode in site 8 fell within the Koty reactivation data field, whereas the data points of the transitional episode in site 9 scattered beyond the Koty reactivation data field. Data points of the transitional episode in site 27 marked a trend of changing components from the Koty reactivation by new components that were characteristic of the Murino reactivation. Responses of groundwater parameters of site 27 were the most sensitive to seismic reorganizations.

7 Temporal *AR* variations in 2012–2014

While analyzing *AR* variations in groundwater during 2012–2014 (Fig. 9), four phases were distinguished on diagrams of sites during every seismic reactivation: 1) an initial phase *a* with earthquake epicenters remote from the Kultuk area, 2) an intermediate phase b with earthquake epicenters in or near the Kultuk area, 3) a final phase *c* with new remote earthquake epicenters, and 4) an aseismic phase *d*.

For the initial sample of site 9 (Fig. 9(a)), the lowest *AR* of 2.44 for the component I_3 was obtained. The subsequent five samples taken during four months showed a persistently increasing *AR* to a maximum value of 2.56 of the component I_1. The lowest and highest *AR* values corresponded to the major and final events of the Tolbazikha reactivation. Afterwards, a sequential of more than a 2.5-month period of decreasing *AR* to a minimum value of 2.47 was recorded by five samples.

Taking into account the 4-month rise of an *AR* in site 9 in 2012, one can connect a low value (2.44) of the first taken sample of this sequence with the phase I*b* of the Tolbazikha reactivation. Similarly, minima of *AR* values were recorded in the phase II*b* of the Koty reactivation and in the phase III*b* of the Murino reactivation. Consequently, each of three seismic reactivations (i.e., phases I*b*, II*b*, and III*b*) had a groundwater signal in site 9 in an *AR* minimum.

The Koty seismic reactivation began with the major event of January 1, 2013, which occurred at the Obruchev fault zone over 120 km from the Kultuk area. The *AR* of site 9 was minimal and was characterized by an increasing, decreasing, and then increasing pattern during phase II*a*. The elevated values of the isotopic ratio (separated by a minimum) corresponded to two events with epicenters in the Kultuk area (phase II*b*). The maximum *AR*, displayed after the June 7, 2013 earthquake (phase II*c*), accompanied the final seismic events of the Koty reactivation.

The Murino reactivation that began on August 11, 2013, with an earthquake over 120 km from the Kultuk area, was characterized by alternating at least three highs and lows of *AR* at the first half of the phase III*a* in site 9. A maximum *AR* of 2.62 was reached in the second half of phase III*a* and was retained from January 21 to February 1, 2014. Subsequently, on February 4, 2014, there was a seismic event near the Obruchev fault that was reflected in the minimum *AR* (2.46) from February 6 to February 16, 2014. There was a new increase of *AR* values maximized at 2.62 and a decrease ranging from 2.49–2.54 (March 16 to April 3, 2014), which initiated a new event that occurred on March 19, 2014, with the epicenter located near the Kultuk village. Further reduction of the *AR* to a minimum of 2.43 from April 9 to April 27, 2014 was accompanied by a major earthquake of the reactivation on April 25, 2014. After this event, there was an intermediate *AR* that accompanied the final earthquake on July 20, 2014, when the epicenter was near the Obruchev Fault.

In phase I*b*, the *AR* of site 8 changed in antiphase with respect to the *AR* of site 9 (Fig. 9(b)). During seismic quiescence (phase I*d*), *AR* variations differed. During the Koty seismic reactivation, high-amplitude *AR* variations were followed with low-amplitude variations. The maximum value observed on October 21, 2013 from site 8, corresponding to the maximum of site 9, occurred during the second half of the phase III*a*. Decreasing and increasing *AR* was then recorded at site 8. The event of March 19, 2014 occurred at the beginning of the descending *AR* curve that yielded the deepest low of this site as a reflection of the major earthquake of the Murino reactivation on April 25, 2014. After this event, an intermediate *AR* accompanied the final earthquake of July 20, 2014.

From comparisons of data obtained in sites 8 and 9, it is inferred that *AR* fluctuations were inconsistent in the Tolbazikha and Koty reactivations. The initial stage of the Murino reactivation was characterized by mutual harmonization of fluctuations in the middle and final stages (in the first half of 2014). Site 27 shows a noticeable decrease of an *AR* from the Koty to Murino reactivation. *AR* oscillation amplitudes were relatively high in the phases II*a*, II*c*–*d*, III*a*, III*c*, and III*d*, but decreased during phases II*b* and III*b* (Fig. 9(c)).

8 Temporal variations of [U] in 2012–2014

Peaks of [U] occurred during different phases of seismic reactivations (Fig. 10). In site 9, a maximum [U] (0.22 μg/L) occurred in phase I*c*. It was displayed after the second major earthquake of this reactivation, the epicenter of which was near the Obruchev fault, before a small event on September 12, 2012 at the Tolbazikha epicenter cluster. In site 8, elevated [U] (3.4–3.5 μg/L) was measured in the

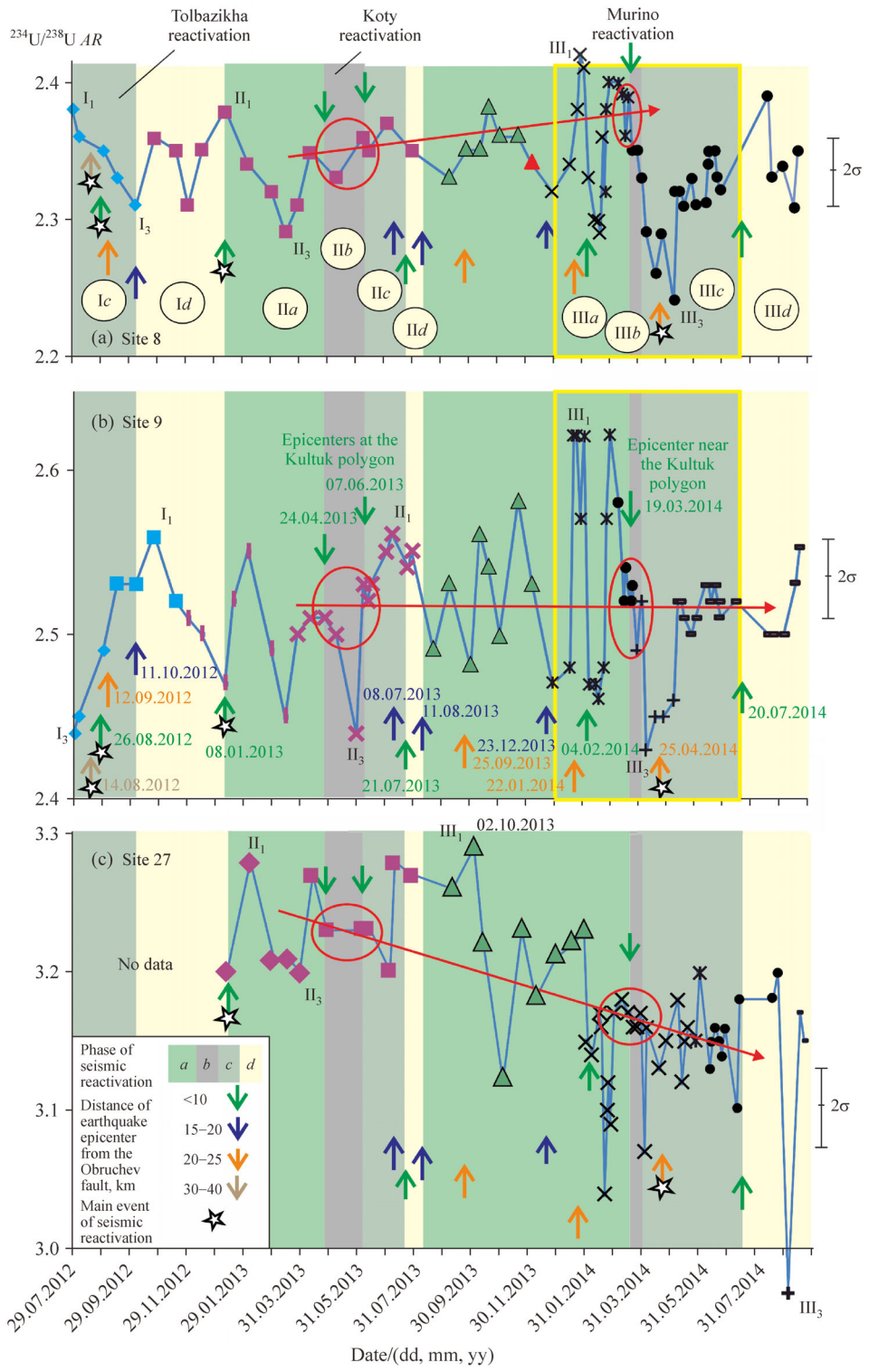

Fig. 9 Temporal *AR* variations in groundwater from sites 9 (a), 8 (b), and 27 (c) in the context of seismic reactivations in the western part of the South Baikal Basin. Symbols as in Fig. 8. The extreme components of seismic reactivations are indicated for each site. Red ellipses mark data points that correspond to the phases II*b* and III*b*, when seismic events occurred in the Kultuk area or its vicinity. Red arrows indicate trends of isotope ratios fixed at the phases II*b* and III*b*. The yellow rectangles on panels *a* and *b* indicate the interval (first half of 2014), in which *AR* oscillations in sites 9 and 8 were mutually consistent. One bar on the abscissa axis corresponds to one month.

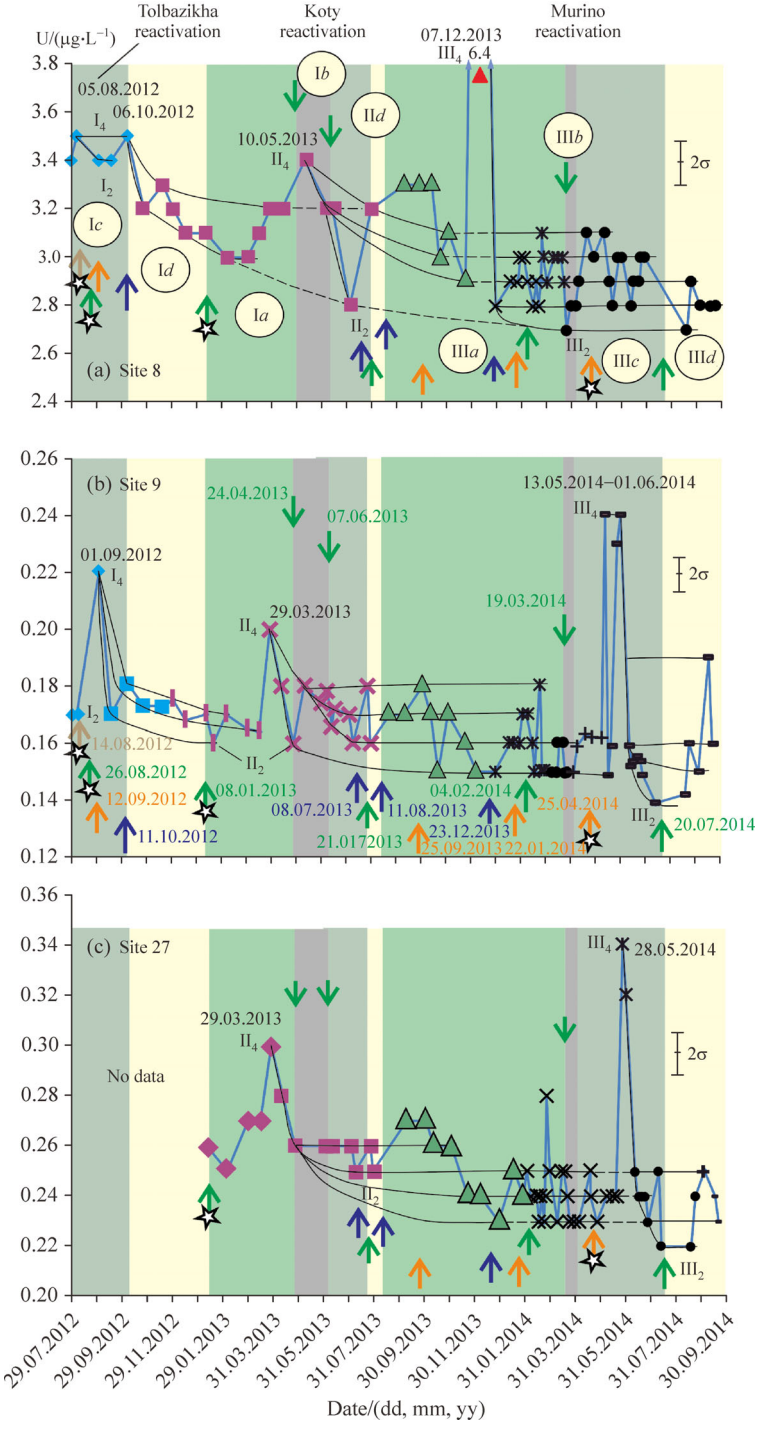

Fig. 10 Temporal variations of [U] in groundwater from sites 9 (a), 8 (b), and 27 (c) in the context of seismic reactivation in the western part of the South Baikal Basin. Symbols of data groups as in Figs. 8 and 9. In panel (a), the phases of small seismic reactivations from I*c* to III*d* that occurred after strong reactivation from 2007–2010, are marked within circles. Green arrows pointing down show dates of earthquakes that occurred in the Kultuk area (Fig. 5), arrows of four different colors directing up indicate dates of earthquakes that occurred outside the area at different distances from the Obruchev fault (Fig. 11). Maximum [U] is followed with the fan of branches with the lower [U]. One bar on the abscissa axis corresponds to one month.

final stage of the Tolbazikha reactivation in response to its major events on August 14, 2012 and August 26, 2012. In the aseismic interval (phase I*d*), [U] decreased to 3.0–3.3 μg/L.

During the next (Koty) seismic reactivation, a [U] maximum of 0.20 μg/L occurred in site 9 on March 29, 2013 simultaneously with a maximum of 0.30 μg/L in site 27. A [U] maximum (3.4 μg/L) was detected in site 8 on May 10, 2013, during phase II*b*. Samples taken from this site on June 8, 2013 and June 13, 2013 (i.e., after the seismic event occurred in the Kultuk area) showed an initial decrease of [U] to 3.2 μg/L, later decreasing further to 2.8 μg/L.

In the Murino reactivation, low-amplitude variations of a [U] in site 9 were followed by high-amplitude variations. After the occurrence of the local earthquake on March 19, 2014, [U] did not exceed 0.162 μg/L. By May 13, 2013, it increased sharply to 0.24 μg/L, followed by a decrease to 0.149 μg/L on February 23, 2014. By June 1, 2014, [U] again increased to 0.24 μg/L and again sharply decreased between June 12 to June 15, 2014 to 0.152 μg/L with the sample collected on July 14, 2014 at the lowest concentration for this site (0.139 μg/L). This minimum was established before the final earthquake of the Murino reactivation on July 20, 2014. This reactivation yielded U release in site 8 in the middle of phase III*a* (December 7, 2013). A [U] of 6.4 μg/L exceeded the average level of [U] of this site by a factor of 2. After this reactivation, [U] decreased almost to a minimum (2.8 μg/L) and then ranged from 2.7 to 3.1 μg/L. In site 27, a U release of 0.34 μg/L from May 28 to June 1, 2014 corresponded to the end of the interval of high [U] in groundwater from site 9 in May 2014.

9 Discussion

9.1 General remarks

It was inferred from GPS data that blocks of the Siberian platform and Transbaikal diverge in the South Baikal Basin in a NW–SE direction (130°) at a rate of 3.4±0.7 mm/year (Sankov et al., 2014). This divergence causes quasi-periodic seismic reactivations, during which earthquake epicenters migrate within the basin toward the southern coast of Lake Baikal. Quasi-periodic earthquake migrations from the Middle Baikal to the Kultuk area reflect the westward expansions of tensile forces during seismic reactivations. These processes are limited by the transverse Khamar-Stanovoi zone that marked a transition from an extension in the South Baikal Basin to compression in the Tunka Valley.

Prior to earthquake rupture, fluid-saturated microcracks are considered as critical systems that can be monitored with shear-wave splitting (Crampin, 1994; Crampin et al., 2015). An unstable state in a seismically-active region is indicated by both foreshock activity and synchronized oscillations of seismic waves (Sobolev et al., 2005). A change of periodicity was recorded through deformation monitoring of ice cover on Lake Baikal from February to March of 2013 and of rocks in the Talaya edit before the 2008 large earthquake (Bornyakov et al., 2015 and 2017). As stress grew within the ice cover due to its thermal expansion during transition to a critical state, oscillatory deformation amplitudes increased simultaneously with a significantly increasing role of small-period fluctuations. Similar change was revealed through processing of data on monitoring of rock deformations in the Talaya edit during the build-up and rupture of the 2008 Kultuk Earthquake. It was inferred that seismogenic deformation developed with transition to a state of self-organization, and that there was a close relationship between the constituent elements and their coordination. The state of the "self-organized criticality" of the deformation process with a change from large to small oscillation periods was observed two weeks before a large earthquake.

9.2 *AR* variations in groundwater as an indicator of crack opening/closing in an active fault

Independent information on a state of a seismically-active fault is provided by variations of geochemical parameters in a groundwater supply system, among which a $^{234}U/^{238}U$ activity ratio is likely indicative of a state of cracks. An increasing *AR* reflects a process of crack opening accompanied by an enhancement of water circulation and accordingly, the extraction of ^{234}U from a fissured rock or mineral to water. Alternatively, a decreasing *AR* indicates a crack closing resulting in a decrease in water circulation and an extracted quantity of ^{234}U (Rasskazov et al., 2018) (Fig. 11).

In the diagram of $^{234}U/^{238}U$ *AR* vs. $^{87}Sr/^{86}Sr$ (Fig. 12), a data field of groundwater from the Kultuk area is bounded by curves that converge at points corresponding to the end-members E (equilibrium U) and NE (nonequilibrium U). In the former, U is in cyclic equilibrium with an elevated Sr isotope ratio (*AR* = 1.0, $^{87}Sr/^{86}Sr = 0.7205$). In the latter, U shows a nonequilibrium signature with a lower Sr isotope ratio (*AR* = 3.3, $^{87}Sr/^{86}Sr = 0.70534$). Data points distributed between the curves are characteristic of groundwater from mylonites of the suture zone that separates the Achaean basement of the Siberian platform from the younger accreted terranes. Those of groundwater from the Achaean block and younger Slyudyanka metamorphic subterrane are shifted to the right and to the left, respectively (not shown in the diagram).

The more a rock is fractured, the higher *AR* and the lower $^{87}Sr/^{86}Sr$ values are expected in groundwater. A sample from site 27 exhibits the NE end-member of circulating groundwater saturating open cracks. Those from other sites contain an admixture of the E end-member. In a two-component mixing model, loci of curves

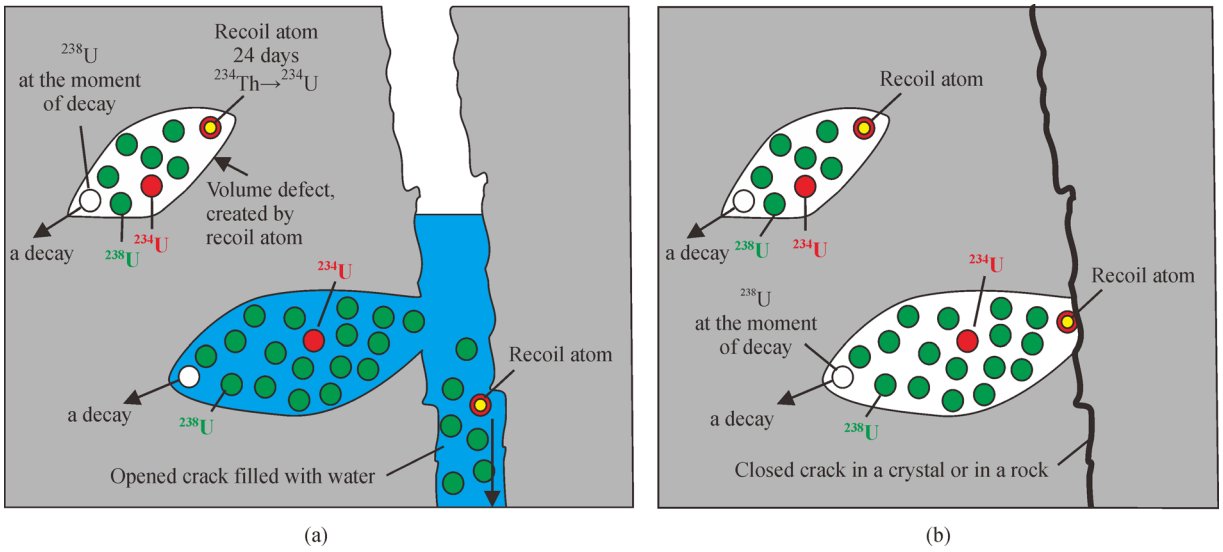

Fig. 11 Explanation of the Cherdyntsev-Chalov effect by crack opening/closing. (a) – recoil atom ^{234}U enrichment of groundwater circulated through open cracks; (b) – no enrichment due to the crack closing that limits the groundwater circulation.

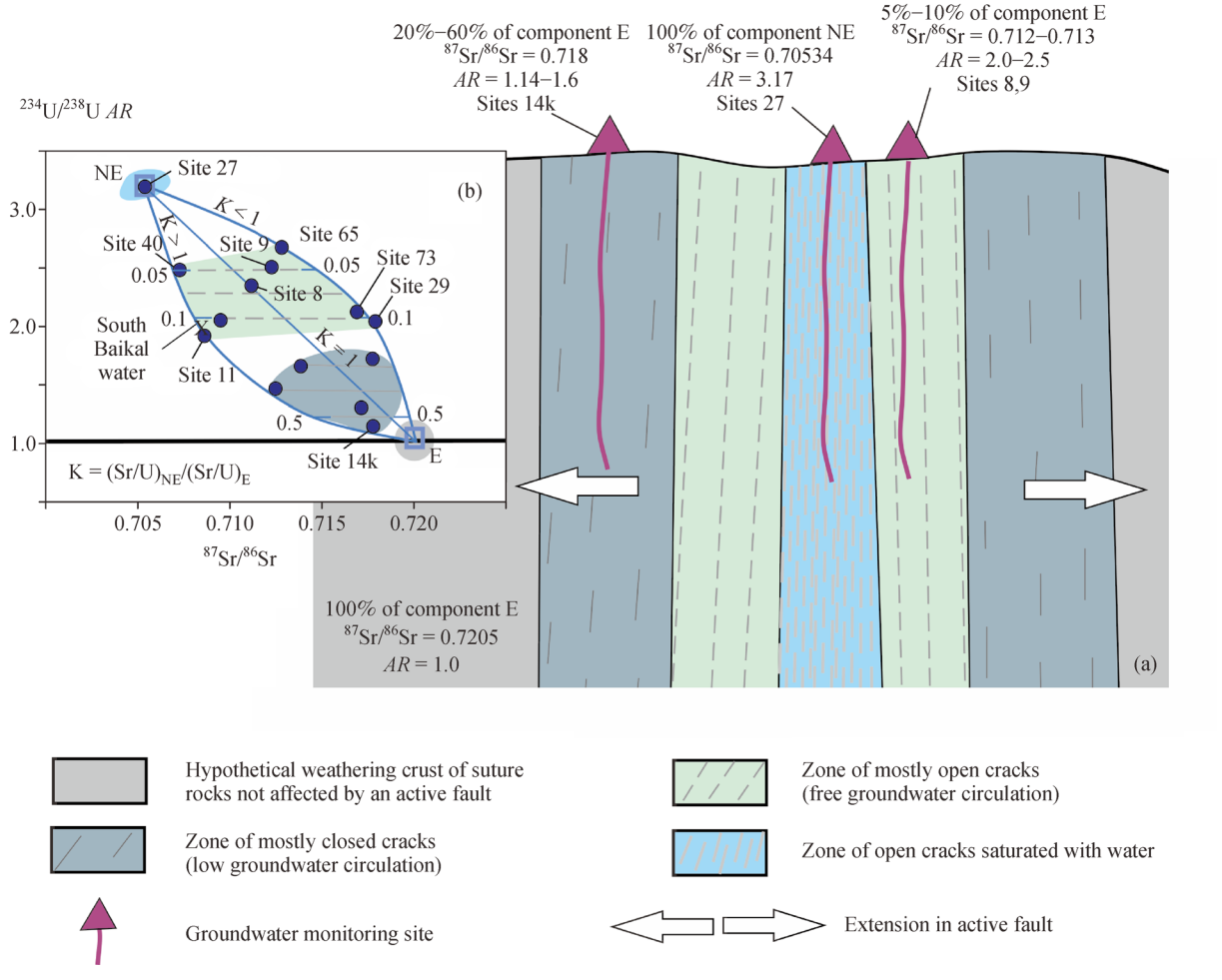

Fig. 12 U–Sr isotope systematics of groundwater from suture rocks in the Kultuk area. (a) – model for end-member mixing on the diagram $^{234}U/^{238}U$ *AR* vs. $^{87}Sr/^{86}Sr$; (b) – subdivision of monitoring sites in terms of water circulation control by opened and closed cracks in an active fault. The end members: E – with equilibrium U, NE – with nonequilibrium U.

reflect variations of the coefficient $K = (Sr/U)_{NE}/(Sr/U)_E$. A sample from site 8 corresponds to $K = 1$. A sample from site 9 is shifted to the model region with $K < 1$. The samples of these two sites represent free-circulating water from a zone of primarily open fractures in an active fault with the E component admixture less than 10%. These samples differ from those that exhibit a hindered circulation, in which the component E admixture ranges from 20 to 60%. The maximum content of this component is measured in a sample from site 14k. In terms of U–Sr isotope systematics, groundwater with $K > 1$ is comparable to deep water from Southern Baikal (Table 3).

9.3 Application of hydroisotopic data

Three of six seismic reactivations that occurred in the western part of the South Baikal Basin from 2003 to 2014 were covered by monitoring of an *AR* in the groundwater in the Kultuk area. Moreover, after migration of seismic activity from the western to central part of the Obruchev Fault, a response of the *AR* in the groundwater was received for a remote large earthquake on September 5, 2015 that was spatially related to the reactivation of the northeastern fragment of this boundary fault. The obtained data set is a basis for substantiation of the method for recording a state of a seismically active fault from *AR* groundwater responses to opening/closing crack variations. Although both elemental and isotopic variations in groundwater were recorded, [U] in groundwater had no direct correlation with phases of seismic reactivations and likely responds to different hydrogeological factors. An analysis of these variations is beyond the scope of this paper.

The high and low *AR* values in groundwater from monitoring sites are indicative for identification of areas with predominantly opened or closed cracks, whereas temporal *AR* variations show superimposed quasi-periodically oscillated opening/closing effects. Each site exhibits integral effects that change over time depending on progressive crack opening (increasing *AR*), or crack closing (decreasing *AR*). The role of crack closure increases within the Kultuk area westwards. Relative *AR* variations in groundwater from monitoring sites responded to deformation along the Obruchev Fault that accompanied earthquakes of the energy classes $K = 8.6–11.0$ in the western part of the South Baikal Basin.

Sites in the Kultuk area yield different information about the course of deformation along the Obruchev Fault zone. Each is a type of "deformation sensor," into which a local volume of fissure water is involved. The deformation mode recorded by one site can be consistent, or conversely, sharply dissonant with the deformation mode recorded by another site. Among 42 sites, the maximum *AR* (the largest integral effect of crack opening) was registered on site 27. Integral effects of crack opening in other sites were lower.

9.4 Hydroisotopic responses to the March 19, 2014 ($K = 9.2$) earthquake near the Kultuk area and comparison with the results of deformation-temperature monitoring

For comparisons of monitoring results in different sites of the Kultuk area, we recalculated data to Delta values that show a degree of *AR* deviations from a median:

$$\text{Delta } AR = 100 \times (AR_{\text{measured}} - AR_{\text{median}})/AR_{\text{median}}.$$

Precursor and rupture activity during the March 19, 2014 earthquake near the Kultuk area was clearly designated by *AR* responses in groundwater from site 14k (location in Fig. 7). The dominant Delta *AR* values of approximately –2.1, in comparison to an *AR* median of 1.165, reflected a crack closure state. This parameter continued to decrease from the earthquakes on January 22, 2014 and February 4, 2014, reaching a minimum (–6.5) on February 23, 2014. A Delta *AR* value of the next sample, taken on March 19, 2014 (three days after the earthquake), was maximal (+ 6.5), followed by a decrease on April 5, 2014 (to –3.9).

Deformation monitoring in the Talaya adit (location shown in Fig. 7) revealed signs of instability (short multi-amplitude deformation impulses) after an earthquake on February 4, 2014 that occurred near the Obruchev Fault. These signals were followed by deformations on March 2, 2014, which increased by an order of magnitude without displaying any perceptible earthquake. This unstable state with short deformation pulses changed by a notable deformation increase (approximately 1.5 times) on March 18, 2014, accompanied by a local earthquake in the Kultuk area the next day, March 19, 2014 ($K = 9.2$), with a maximum observed on March 21, 2014. At the onset of short deformation pulses after the earthquake of February 4, 2014, rock temperatures in the Talaya adit

Table 3 U and Sr concentrations and isotope ratios in groundwater from the Kultuk area and in deep water from Lake Baikal

Sample location	$U/(\mu g \cdot L^{-1})$	$^{234}U/^{238}U$ *AR*	PRE (1σ) /%	$Sr/(\mu g \cdot L^{-1})$	$^{87}Sr/^{86}Sr$	±2σ
Site 8	3.30	2.33	0.72	123	0.711328	0.000010
Site 9	0.17	2.53	0.82	158	0.712377	0.000009
Site 27	0.27	3.26	0.79	65	0.705341	0.000009
Site 14k	0.42	1.14	1.10	140	0.717888	0.000009
Southern Baikal	0.45	1.96	0.80	99	0.708629	0.000009

Note: PRE–percent relative error.

increased. One temperature anomaly began on February 18, 2014, reaching a maximum on February 21, 2014. A water sample, taken from site 14k on February 23, 2014, showed a Delta *AR* minimum value. Conversely, the deepest temperature minimum of March 19, 2014 corresponded to a pronounced Delta *AR* maximum and was accompanied by an earthquake (Figs. 13 and 14).

The temperature anomaly likely resulted from friction

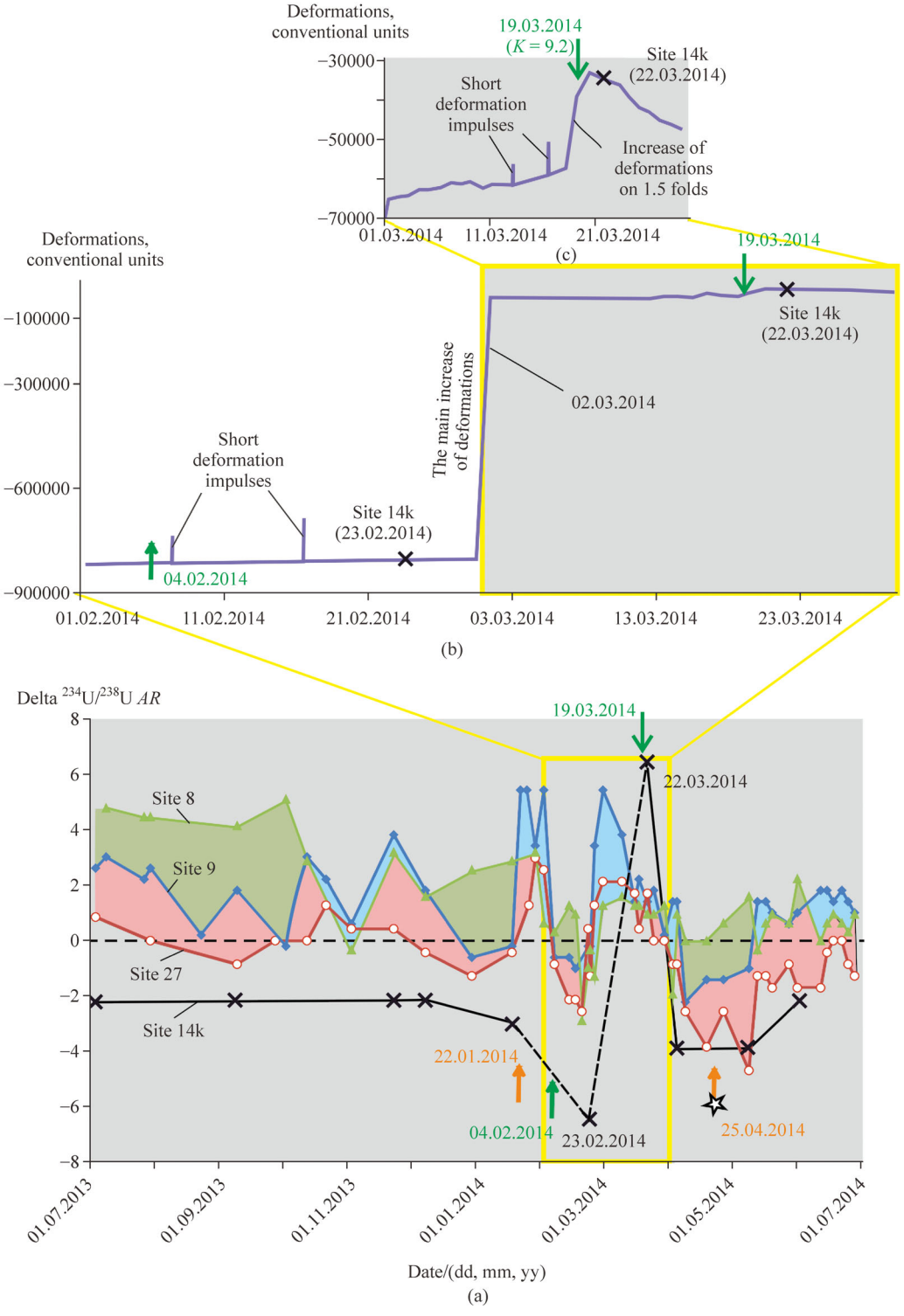

Fig. 13 Temporal variations of a Delta *AR* in groundwater from sites 9, 8, 27, and 14k (a) in comparison to temporal variations of rock deformation recorded in the Talaya adit in a first approximation (b) and with a high resolution (c). The values of an *AR* median are accepted for a 6-year time interval of observations: site 9 – 2.485, site 8 – 2.35, site 27 – 3.13, site 14k – 1.165.

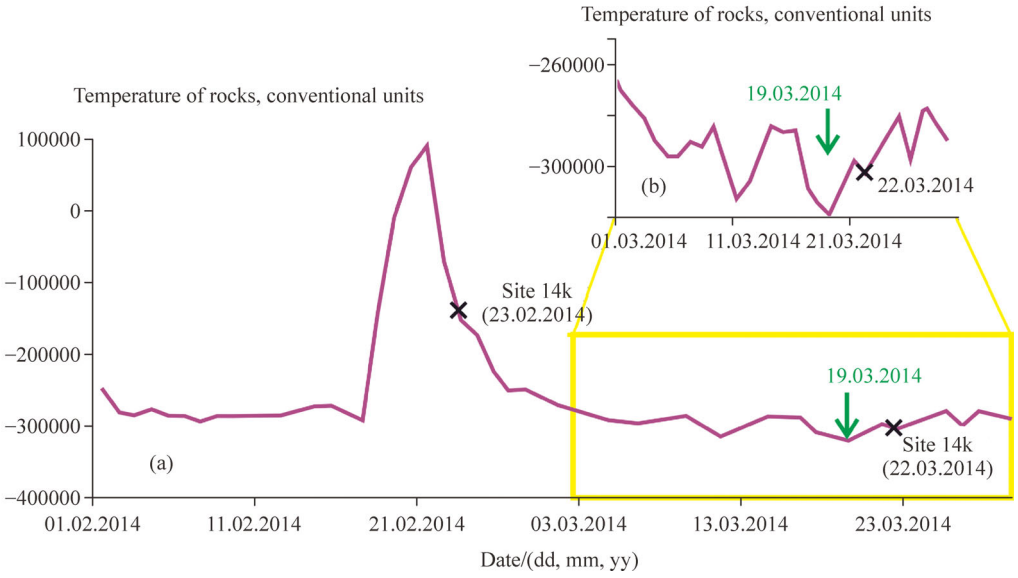

Fig. 14 Variations of temperature in rocks of the Talaya adit recorded in a first approximation (a) and with a high resolution (b) as compared to timing of an earthquake on March 19, 2014 and sampling of site 14k on February 23, 2014 and March 22, 2014.

due to compression that contributed also to a crack closure with a relative decreasing Delta *AR* in groundwater from site 14k. No perceptible earthquakes occurred during the compression phase. The temperature decrease reflected heat losses during extension. It was the extension phase that led to crack opening, resulting in water circulation in site 14k, and to a seismic shock on March 19, 2014.

In contrast to low values of a Delta *AR* in site 14k, those in other monitoring sites plotted close to a median (site 27) or above it (sites 8 and 9). The Obruchev Fault instability of early 2014 was expressed in decreasing Delta *AR* values in all three sites with partial transition to negative values. During earthquakes of January 22, 2014 and February 4, 2014, Delta *AR* parameters in these sites showed maxima followed by minima that coincided with the minimum of February 23, 2014 in site 14k. Delta *AR* parameters subsequently rose. The high values corresponded to the local earthquake of March 19, 2014.

The consistent hydroisotopic and deformation-temperature records indicate the beginning of a local earthquake build-up during seismic events in the inundated area of Southern Baikal from January 22 to February 4, 2014. The instability in the Obruchev Fault zone in the Kultuk area was first expressed by compression (crack closing) on February 23, 2014, followed by a sharp deformation increase on March 2, 2014, which promoted extension with crack opening and water circulation from February 22 to March 10, 2014, resulting in a seismic event on March 19, 2014.

When evaluating *AR* data from site 9 for the Murino reactivation (Fig. 15(a)), temporal steps of close values within error are separated by rapid transitions. From January 1 to June 30, 2014, the step intervals increased from 10 to 43 days. A small earthquake on March 19, 2014 occurred at the beginning of the intermediate step with an *AR* value of ~2.52. The major event of the Murino reactivation of April 25, 2014 was in the middle of the lowest step with an *AR* value of ~2.44. Similar alternating *AR* maxima and minima of site 8 (Fig. 15(b)) showed additional intermediate data points between the temporal steps.

9.5 Hydroisotopic responses to the remote Goloustnoe earthquake of September 5, 2015 ($K = 12.4$)

As compared to small seismic shocks in the Kultuk area, the larger remote earthquake of September 5, 2015 ($K = 12.4$), called the Goloustnoe earthquake, was reflected in a longer interval of *AR* responses. The graphs, compressed along the time axis (Figs. 16 and 17), demonstrate changes of extreme isotope ratios as indicators of the opening/closing of cracks in the Obruchev Fault that had preceded this earthquake since 2013.

Long-term build-up of the Goloustnoe Earthquake was well recorded in site 27. In the initial observation interval of 2013, *AR* values in the groundwater of this site were elevated and fluctuations of the parameter were small. Over time, the amplitudes of *AR* variations increased with decreasing *AR* values up to a minimum in the aseismic interval that occurred over the entire length of the Obruchev Fault from July 20, 2014 to January 13, 2015. After this interval, *AR* values slightly increased at large amplitudes of short-period variations. Subsequently, between April 25, 2015 and November 21, 2015, the high-amplitude, short-period variations of this parameter were followed by low-amplitude variations for seven

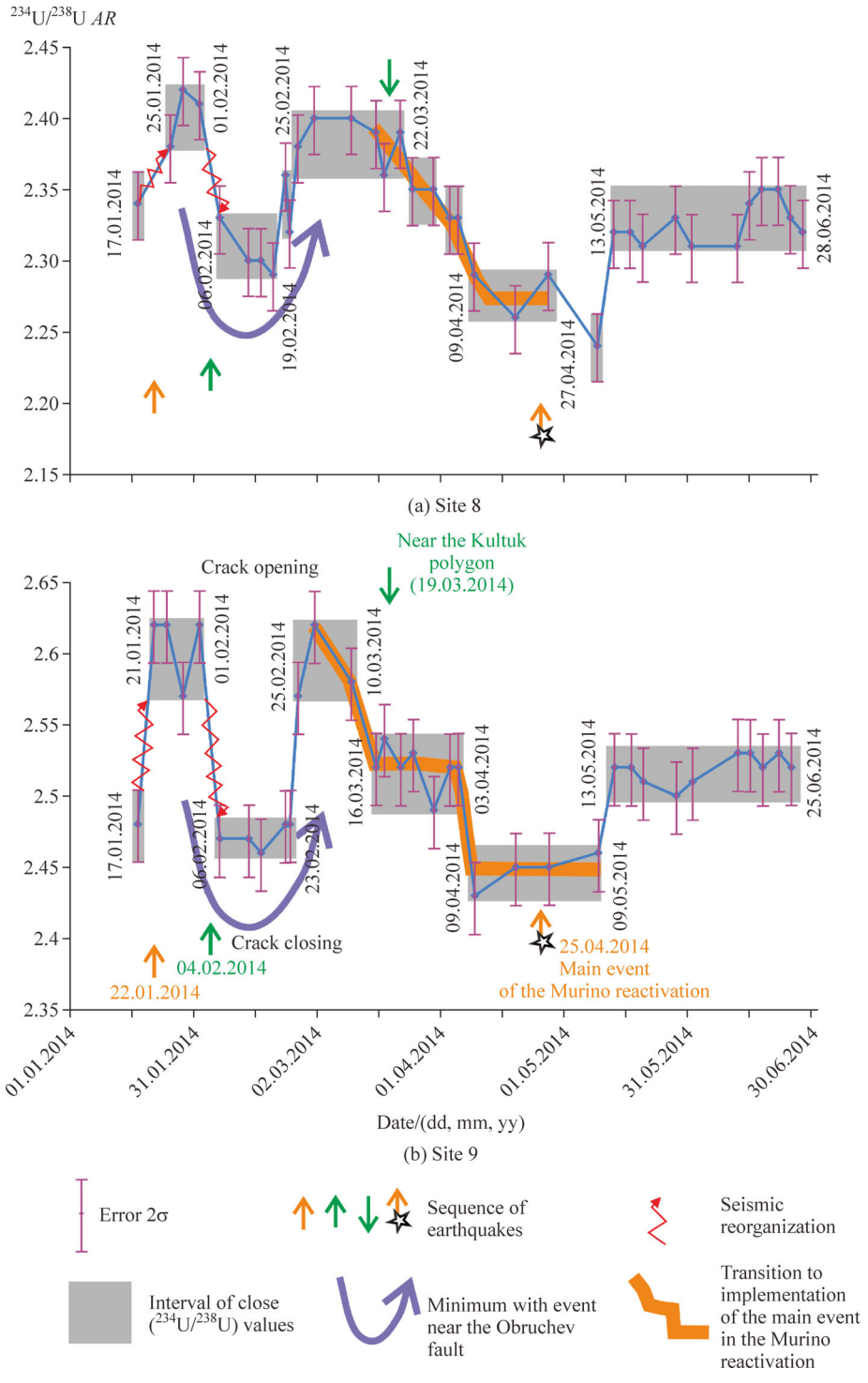

Fig. 15 Relationship between *AR* steps in sites 8 (a) and 9 (b) during the Murino reactivation (during the first half of 2014). One step designates a time interval in which *AR* values are comparable to each other within error.

months, during which a large earthquake occurred on September 5, 2015. The uniform small amplitudes suggest a seismically dangerous state of the Obruchev Fault. An *AR* level of 3.18, measured in site 27 during this time, corresponded to a previous earthquake in the Kultuk area on March 19, 2014 (Fig. 16). The seismic hazard interval was followed with *AR* decrease and a transition to relatively wide fluctuations, which continued until the end of the monitoring.

AR responses to the Goloustnoe Earthquake build-up in sites 8 and 9 (Fig. 17) differed from the response in site 27. The minimum response in site 8 was reached before the

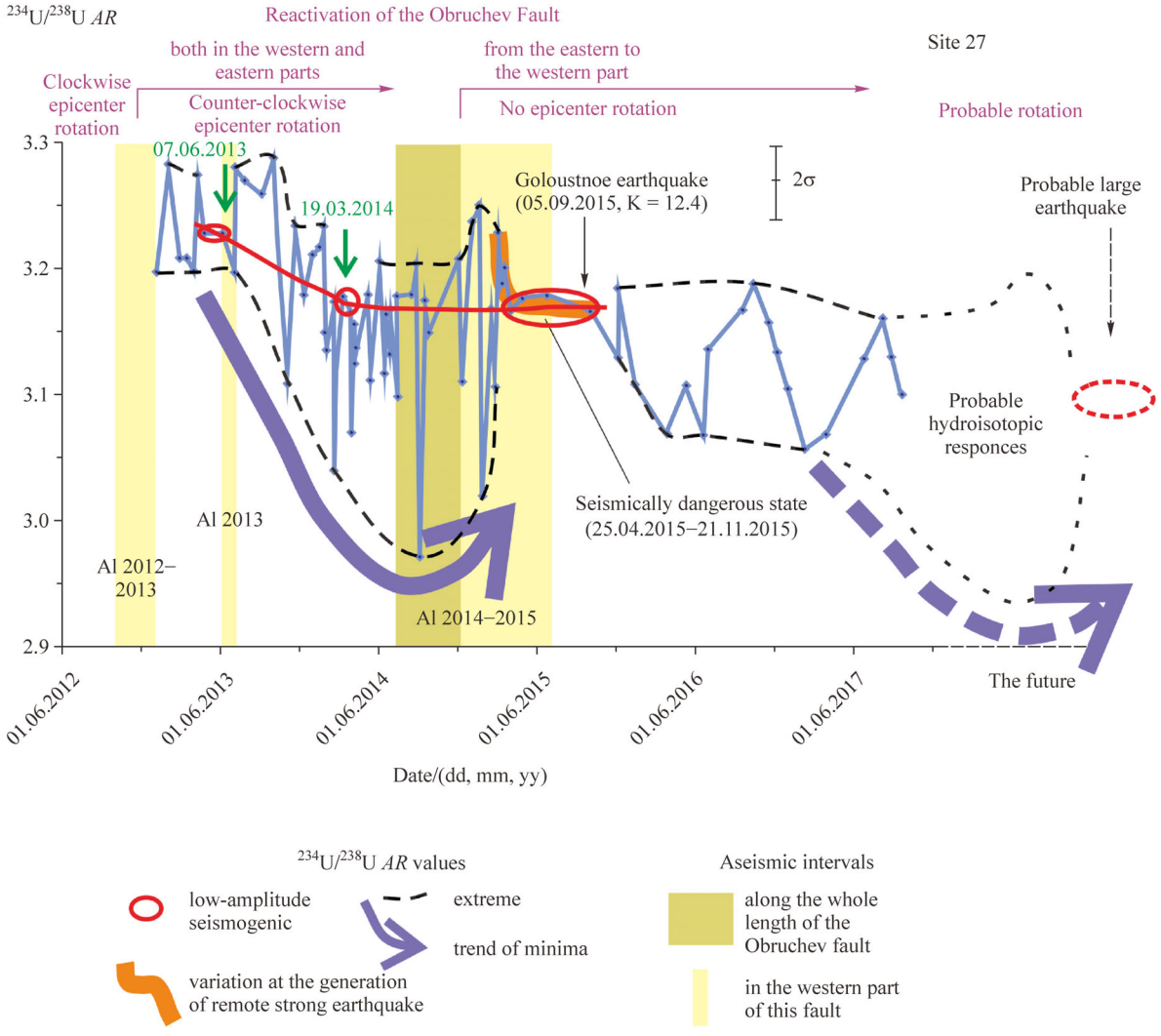

Fig. 16 Temporal variations of an *AR* in groundwater of site 27 from 2013 to 2017 and proposed future hydroisotopic responses to build-up and occurrence of a probable large earthquake.

aseismic interval of the entire Obruchev Fault, whereas the minimum of site 9 was reached after this interval. The subsequent transition of the Obruchev Fault to a seismic state was accompanied by asynchronous *AR* variations at these sites, while synchronization occurred at the end of the seismic state. In 2015, sites 8 and 9 showed a transition from high- to low-amplitude *AR* fluctuations, similar to site 27. In site 8, the low-amplitude interval (March 7 to November 21, 2015) was the longest (8.5 months), whereas in site 9, the interval lasted only 5 months (June 23 to November 21, 2015). In contrast to site 27, low-amplitude intervals of sites 8 and 9 were followed by an increasing *AR*. The prolonged interval of this parameter reduction in site 27 corresponded to the interval of an increasing *AR* in site 8. Transitions from high- to low-amplitude *AR* fluctuations, accompanied by small seismic events in the Kultuk area and by the remote large earthquake, are also clearly revealed in the combined $AR_{9/8}$. In all the diagrams, hydroisotopic responses to a large seismic event differed from small events in the Kultuk area by recording longer intervals between the earthquake build-up and the high-amplitude fluctuations that preceded low-amplitude co-seismic effects.

9.6 Probable scenarios for the development of seismically-dangerous processes in the South Baikal Basin and expected hydroisotopic responses

During the period of hydroisotopic monitoring in the Kultuk area, two signals of build-up to a probable large earthquake in the South Baikal Basin are noted: 1) a specific (K = 12.4) seismic event in the Goloustnoe epicenter cluster on September 5, 2015, and 2) diagonal migration of earthquake epicenters from the northeastern fragment of the Obruchev Fault along the Goloustnoe-Murino line from 2015–2017 and along the Listvyanich-

noe-Posolskaya Bank in 2018 (Figs. 4 and 18). More than 21 months have passed since the preparation of this manuscript, during which time no earthquake activity has occurred in South Baikal. The epicenter location of a potential future large earthquake (Fig. 18) depends on seismic signals that may reveal migrating seismic activity in 2020 or later. An approaching large earthquake should be recorded through hydroisotopic and deformation-temperature monitoring in the Kultuk area, even in absence of seismicity.

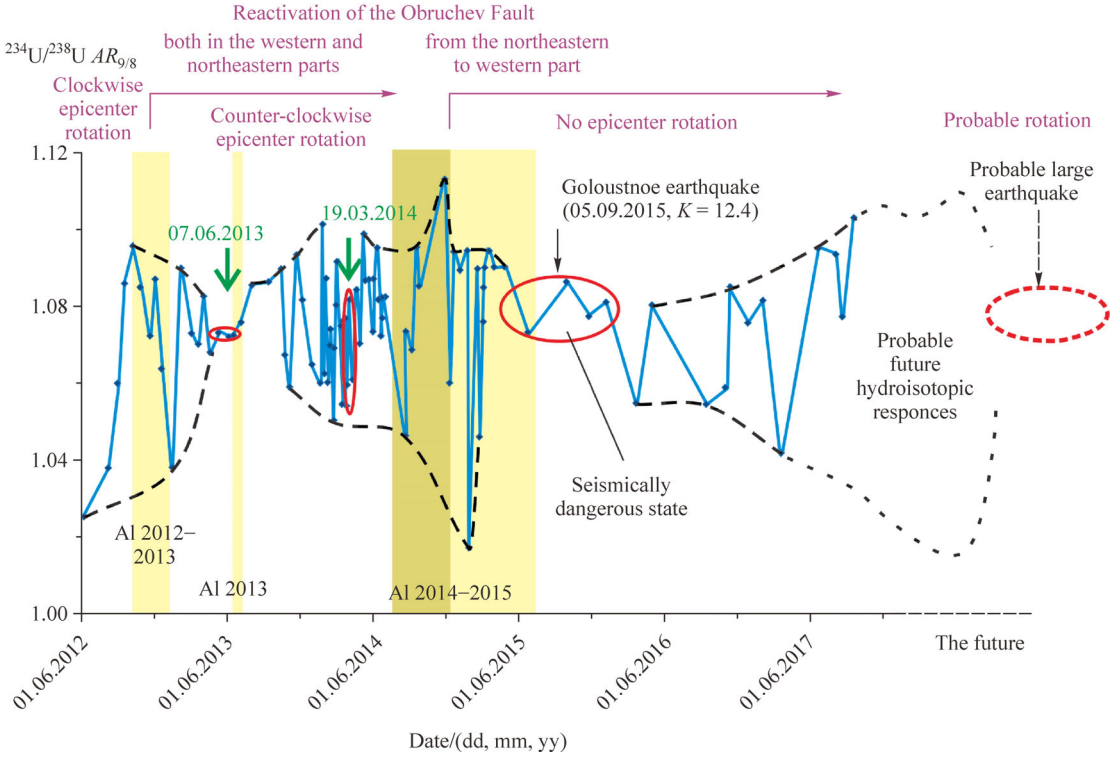

Fig. 17 Temporal variations of an *AR* site 9/site 8 in groundwater from 2012 to 2017 and proposed future hydroisotopic responses to buildup and occurrence of a probable large earthquake. Symbols as in Fig. 16.

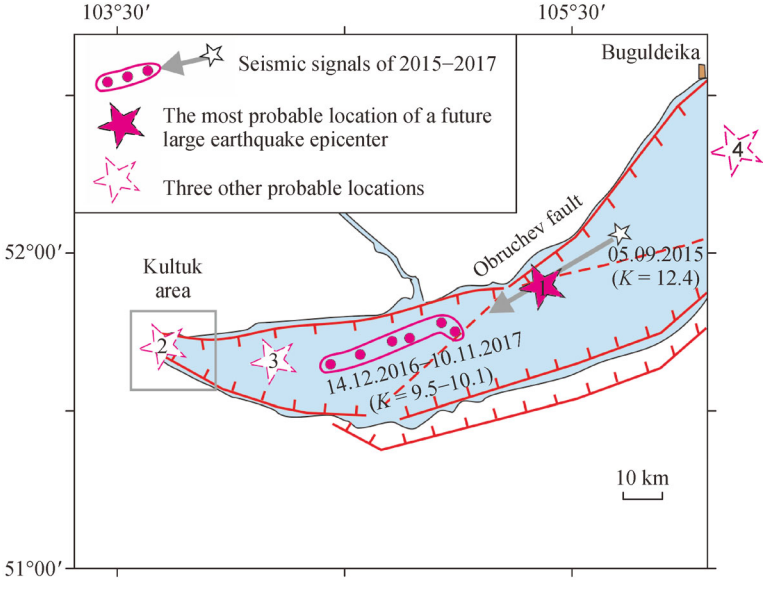

Fig. 18 Options of a probable large earthquake epicenter in the South Baikal Basin (explanations in the text). Symbols as in Fig. 4. Four probable positions of the epicenter: 1 – central part of the Obruchev Fault, 2 – Kultuk area, 3 – lake area near Kultuk, 4 – Middle Baikal.

The results of this work suggest that small and large earthquakes may be indicated by transitions in *AR* from high-amplitude, inconsistent fluctuations to low-amplitude, consistent fluctuations. A pre-seismogenic state is expressed by a significantly decreased *AR* in groundwater of the Kultuk area (effect of crack closure), followed by a transition to an *AR* maximum (effect of crack opening).

Southwestern termination of the 2007 Peschanaya-Snezhnaya earthquake band (Fig. 4(a)) almost reached the SW boundary fault that led to a reactivation of a block between this fault and the western fragment of the Obruchev Fault with the rupture of the 2008 Kultuk Earthquake. Unlike the 2007 Peschanaya-Snezhnaya earthquake band, the 2015–2017 Goloustnoe-Murino earthquake line of the phase D1 was narrower and situated closer to the western fragment of the Obruchev Fault (Figs. 4(b) and 6(b)). The phase D2 complicated the development of seismic processes as compared to the build-up of the 2008 Kultuk Earthquake.

It is likely that future migration of earthquake epicenters will proceed from the Murino epicenter cluster to the Kultuk area with a subsequent rupture of a large earthquake either in the Kultuk area or in the adjacent Lake Baikal area, similar to the 2008 Kultuk Earthquake scenario (the probable epicenters 2 and 3 in Fig. 18). It is noteworthy, however, that seismic activity shifted from the western part of the South Baikal Basin toward the Middle Baikal after 2014. This indicates the possibility of a large earthquake rupture in the central portion of the Obruchev Fault or in the vicinity of its northeastern termination, beyond the eastern border of the scheme shown in Fig. 18 (the probable epicenters 1 and 4). Taking into account the inheritance factor of the seismic process development, however, the potential for a large earthquake in the central part of the Obruchev Fault seems the most probable (option 1 in Fig. 18).

10 Conclusions

An analysis of earthquake epicenters of the South Baikal Basin reveals a quasi-periodic character of seismic reactivation. The largest 1999 South Baikal (M_W = 6.0; K = 14.6) and 2008 Kultuk (M_W = 6.3, K = 15.9) earthquakes corresponded to seismic intervals from 1994–2003 and 2003–2012. Seismic reactivation of the latter was exhibited by concentration of seismicity along the Obruchev Fault and the SW boundary fault of the basin. During this reactivation, epicenters rotated clockwise. From 2013–2014, epicenters were localized along the Obruchev Fault and rotated counter-clockwise with subsequent concentration along the Goloustnoe-Murino line without any rotation.

Since mid-2012, the $^{234}U/^{238}U$ activity ratio has been monitored in the groundwater of the Kultuk area. Recorded *AR* temporal variations demonstrated that crack opening/closing responded to the seismogenic state in active faults of the South Baikal Basin. Both local seismic events of April 24, 2013, June 7, 2013, and March 19, 2014 in the Kultuk area, and also the remote larger Goloustnoe earthquake of September 5, 2015, are evident in hydroisotopic responses expressed by a transition from disordered, high-amplitude to consistent, low-amplitude *AR* fluctuations in groundwater from different sites of the Kultuk area.

The hydroisotopic responses to seismic events and recorded data on deformation and temperature variations in rocks are informative for a comprehensive assessment of the seismogenic potential of active faults in the South Baikal Basin. The patterns of *AR* variations in groundwater from the sites of the Kultuk area can serve as the basis for prediction of a large seismic event in the Basin. The central part of the Obruchev Fault is the most likely location among the four options for the occurrence of a large seismic event.

Acknowledgements We are grateful to Drew Coleman for critical reading and correction of the manuscript and also to anonymous reviewer for constructive comments. In analytical work, we used an Agilent 7500 ce quadrupole mass spectrometer in the collective use center "Ultramicroanalysis" (Limnological institute of the Siberian Branch of the Russian Academy of Sciences, Irkutsk) and a Finnigan MAT 262 mass spectrometer of the collective use center "Geochronology and Geodynamics" (Institute of the Earth's crust SB RAS, analyst N.N. Fefelov). The work has been prepared with the financial support of Russian Science Foundation (grant 18-77-10027).

References

Belichenko V G, Reznitsky L Z, Makrygina V A, Barash I G (2006). Terranes of the Baikal–Khubsugul fragment of the Central Asian mobile belt of Paleozoides: state of a problem. Geodynamic evolution of the lithosphere in the Central Asian mobile belt. In: Conference Proceedings 4(1) of an Ocean to a Continent. Irkutsk: Institute of the Earth crust SB RAS, 37–40

Boldina S V, Kopylova G N (2017). Effects of the January 30, 2016, *M*w = 7.2 Zhupanovsky Earthquake on the water level variations in wells YuZ-5 and E-1 in Kamchatka. Geodynamics & Tectonophysics, 8(4): 863–880

Bornyakov S A, Miroshnichenko A I, Salko D (2015). Diagnostics of pre-seismogenic state of heterogeneous environments according to the deformation monitoring. Dokl Earth Sci, 468(1): 84–87

Bornyakov S A, Ma J, Miroshnichenko A I, Guo Y, Salko D V, Zuev F L 2017. Diagnostics of meta-instable state of seismically active fault. Geodynamics & Tectonophysics 8 (4): 989–998

Cizdziel J, Farmer D, Hodge V, Lindley K, Stetzenbach K (2005). $^{234}U/^{238}U$ isotope ratios in groundwater from Southern Nevada: a comparison of alpha counting and magnetic sector ICP-MS. Sci Total Environ, 350(1-3): 248–260

Chabaux F, Granet M, Larqué P, Riotte J, Skliarov E V, Skliarova O, Alexeieva L, Risacher F (2011). Geochemical and isotopic (Sr, U)

variations of lake waters in the Ol'khon region, Siberia, Russia: Origin and paleoenvironmental implications. C R Geosci, 343(7): 462–470

Chalov P I (1975). Isotope Fractionation of Natural Uranium. Frunze: Ilim

Chebykin E P, Goldberg E L, Kulikova N S, Zhuchenko N A, Stepanova O G, Malopevnaya Y A (2007). Method of determination of the isotopic composition of authigenic uranium in the bottom sediments of Lake Baikal. Russ Geol Geophys, 48(6): 604–616

Chebykin E P, Rasskazov S V, Vodneva E N, Ilyasova A M, Chuvashova I S, Bornyakov S A, Seminsky A K, Snopkov S V (2015). The first results of monitoring $^{234}U/^{238}U$ in water from active faults of the western coast of Southern Baikal. Dokl Earth Sci, 460 (4): 464–467

Cherdyntsev V V (1969). Uranium-234. Moscow: Atomizdat

Cherdyntsev V V (1973). Nuclear Volcanology. Moscow: Nauka

Chia Y, Chiu J J, Chiang Y H, Lee T P, Liu C W (2008). Spatial and temporal changes of groundwater level induced by thrust faulting. Pure Appl Geophys, 165(1): 5–16

Chipizubov A V, Smekalin O P (1999). Paleoseismodislocations and related paleoearthquakes at the Main Sayan Fault zone. Russ Geol Geophys, 40(6): 936–937

Claesson L, Skelton A, Graham C, Dietl C, Mörth M, Torssander P, Kockum I (2004). Hydrogeochemical changes before and after a major earthquake. Geology, 32(8): 641–644

Crampin S (1994). The fracture criticality of crustal rocks. Geophys J Int, 118(2): 428–438

Crampin S, Gao Y, Bukits J (2015). A review of retrospective stress-forecasts of earthquakes and eruptions. Phys Earth Planet Inter, 245: 76–87

Dobrynina A A, Sankov V A (2008). Destination ripping in earthquake hypocenters as an indicator of a propagating destructive process (Baikal rift system). In: Conference Proceedings 6(1) of Geodynamic evolution of the lithosphere in the Central Asian belt (from ocean to continent). Irkutsk: Institute of the Earth's crust SB RAS, 110–112

Edgington D N, Robbins J A, Colman S M, Orlandini K A, Gustin M P (1996). Uranium-series disequilibrium, sedimentation, diatom frustules and paleoclimate change in Lake Baikal. Earth Planet Sci Lett, 142(1-2): 29–42

Finkel R C (1981). Uranium concentrations and $^{234}U/^{238}U$ activity ratios in fault-associated groundwater as possible earthquake precursors. Geophys Res Lett, 8(5): 453–456

Florensov N A (1968). Baikal Rift Zone and Some Problems of Its Study. Moscow: Nauka, 40–56

Goldberg E L, Grachev M A, Edgington D, Navier J, André L, Chebykin E P, Shulpyakov O I (2001). Direct U–Th dating of the two recent interglacials in the sediments of Lake. Baikal. Dokl Earth Sci, 380(6): 805–808

Halicz L, Segal I, Gavrieli I, Lorber A, Karpas Z (2000). Determination of the $^{234}U/^{238}U$ ratio in water samples by inductively coupled plasma mass spectrometry. Anal Chim Acta, 422(2): 203–208

Hutchinson D R, Golmshtok A J, Zonenshain L P, Moore T C, Scholz C A, Klitgord K (1992). Depositional and tectonic framework of the rift basins of Lake Baikal from multichannel seismic data. Geology, 20 (7): 589–592

Johnson A G, Kovach R L, Nur A (1974). Fluid-pressure variations and fault creep in Central California. Tectonophysics, 23(3): 257–266

King C Y, Koizumi N, Kitagawa Y (1995). Hydrogeochemical anomalies and the 1995 kobe earthquake. Science, 269(5220): 38–39

Levi K G, Babushkin S M, Badardinov A A, Buddo V Yu, Larkin G V, Miroshnichenko A I, Sankov V A, Ruzhich V V, Wong X K, Delvo D, Coleman S (1995). Active tectonics of the Baikal depression. Russ Geol Geophys, 36(10): 154–163

Li B, Shi Z, Wang G, Liu C (2019). Earthquake-related hydrochemical changes in thermal springs in the Xianshuihe Fault zone, Western China. J Hydrol, 579: 124175

Logatchev N A (1974). Sayan-Baikal and Stanovoy highlands. In: Highlands of Pribaikal and Transbaikal. Moscow: Nauka

Maher K, DePaolo D J, Christensen J N (2006). U–Sr isotopic speedometer: fluid flow and chemical weathering rates in aquifers. Geochim Cosmochim Acta, 70(17): 4417–4435

Map of earthquake epicenters in the last ten days (2018). The Baikal Branch of the Geophysical Survey, Irkutsk. Available at www.seis-bykl.ru/index.php?ma = 1

Melnikova V I, Gileva N A, Arefiev S S, Bykova V V, Masalskiy O K (2012). The Kultuk Earthquake in 2008 with M_w= 6.3 in the south of Lake Baikal: spatial-temporal analysis of seismic activity. Izvestiya. Physics of the Solid Earth, 48(11): 44–62

Paces J B, Ludwig K R, Peterman Z E, Neymark L A (2002). $^{234}U/^{238}U$ evidence for local recharge and patterns of groundwater flow in the vicinity of Yucca Mountain, Nevada, USA. Appl Geochem, 17(6): 751–779

Pin C, Zalduegui J F S (1997). Sequential separation of light rare-earth elements, thorium and uranium by miniaturized extraction chromatography: application to isotopic analyses of silicate rocks. Anal Chim Acta, 339(1-2): 79–89

Plastino W, Panza G F, Doglioni C, Frezzotti M L, Peccerillo A, De Felice P, Bella F, Povinec P P, Nisi S, Ioannucci L, Aprili P, Balata M, Cozzella M L, Laubenstein M (2011). Uranium groundwater anomalies and active normal faulting. J Radioanal Nucl Chem, 288 (1): 101–107

Radziminovich N A, Melnikova V I, Sankov V A, Levi K G (2006). Seismicity and seismotectonic deformation of crust in the South Baikal Basin, Izvestiya. Physics of the Solid Earth, 42(11): 44–62

Rasskazov S V, Chebykin E P, Ilyasova A M, Vodneva E N, Chuvashova I S, Bornyakov S A, Seminsky A K, Snopkov S V, Chechel'nitsky V V, Gileva N A (2015). Creating the Kultuk polygon for earthquake prediction: variations of ($^{234}U/^{238}U$) and $^{87}Sr/^{86}Sr$ in groundwater from active faults at the western shore of Lake Baikal. Geodynamics & Tectonophysics 6 (4): 519–553

Rasskazov S V, Ilyasova A M, Chuvashova I S, Chebykin E P (2018). The $^{234}U/^{238}U$ variations in groundwater from the Mondy area in response to earthquakes at the termination of the Tunka Valley in the Baikal Rift System. Geodynamics & Tectonophysics 9(4): 1217–1234

Rasskazov S V, Yasnygina T A, Chuvashova I S, Mikheeva E A, Snopkov S V (2013). The Kultuk Volcano: spatial-temporal change of magmatic sources at the western terminus of the South Baikal Basin between 18 and 12 Ma. Geodynamics & Tectonophysics 4 (2): 135–168

Reddy D V, Nagabhushanam P, Sukhija B S (2011). Earthquake (M = 5.1) induced hydrogeochemical and $\delta^{18}O$ changes: validation of

aquifer breaching-mixing model in Koyna, India. Geophys J Int, 184 (1): 359–370

Riotte J, Chabaux F (1999). ($^{234}U/^{238}U$) activity ratios in freshwaters as tracers of hydrological processes: the Strengbach watershed (Vosges, France). Geochim Cosmochim Acta, 63(9): 1263–1275

Ruzhich V V (1997). Seismotectonic Destruction in the Crust of the Baikal Rift Zone. Novosibirsk: Publishing House of SB RAS

Sankov V A, Lukhnev A V, Miroshnichenko A I, Dobrynin A A, Ashurkov S V, Byzov L M, Dembelov M G, Calais E, Deversher J (2014). Modern horizontal movement and seismic activity south of the Baikal basin (Baikal rift system). Physics of the Earth, 6: 70–79

Shafeev A A (1970). Precambrian of the South-Western Pribaikalye and Khamar-Daban. Moscow: Nauka

Shen C C, Lawrence Edwards R, Cheng H, Dorale J A, Thomas R B, Bradley Moran S, Weinstein S E, Edmonds H N (2002). Uranium and thorium isotopic and concentration measurements by magnetic sector inductively coupled plasma mass spectrometry. Chem Geol, 185(3–4): 165–178

Sherman S I (2009). A tectonophysical model of a seismic zone: experience of development based on the example of the Baikal rift system. Izvestiya. Physics of the Solid Earth, 45(11): 938–951

Sherman S I (2013). Deformation waves as a trigger mechanism of seismic activity in seismic zones of the continental lithosphere. Geodynamics & Tectonophysics 4 (2): 83–117.

Sherman S I (2014). The Seismic Process, and Earthquake Prediction: Tectonophysical Concept. Novosibirsk: Academic Publishing House "Geo"

Shi Z, Wang G, Manga M, Wang C Y (2015). Mechanism of co-seismic water level change following four great earthquakes — insights from co-seismic responses throughout the Chinese mainland. Earth Planet Sci Lett, 430: 66–74

Sobolev G A (1993). Fundamentals of Earthquake Prediction. Moscow: Nauka

Sobolev G A, Lyubshin A A Jr, Zakrzhevskaya N A (2005). Synchronization of microseismic variations within minute range of periods. Izvestiya. Physics of the Solid Earth, 41(8): 3–27

Solonenko, V P (1974). Seismogeology and the problem of prediction of earthquakes. Geology and Geophysics 5: 168–178

Sukhija B S, Reddy D V, Nagabhushanam P, Kumar B (2010). Significant temporal changes in ^{13}C in dissolved inorganic carbon of groundwater related to reservoir-triggered seismicity. Seismol Res Lett, 81(2): 218–224

Timofeev V Y, Kalish E N, Stus Y F, Ardyukov D G, Arnautov G P, Smirnov M G, Timofeev A V, Nosov D A, Sizikov I S, Boyko E V, Gribanova E I (2013). Gravity variations and modern geodynamics southwestern part of the Baikal region. Geodynamics & Tectonophysics 4 (2): 135–168

Tsunogai U, Wakita H (1995). Precursory chemical changes in ground water: Kobe Earthquake, Japan. Science, 269(5220): 61–63

Wang R M, You C F (2013). Uranium and strontium isotopic evidence for strong submarine groundwater discharge in an estuary of a mountainous island: a case study in the Gaoping River estuary. Mar Chem, 157: 106–116

Zverev V L, Dolidze N I, Spiridonov A I (1975). Anomaly of even isotopes of uranium in groundwater of seismically active regions of Georgia. Geochem Int, (11): 1720–1724